RESEARCH ARTICLE

Noncompetitive antagonists induce cooperative AMPA receptor channel gating

Edward Y. Shi*, Christine L. Yuan*, Matthew T. Sipple*, Jayasri Srinivasan, Christopher P. Ptak, Robert E. Oswald, and Linda M. Nowak

Glutamate is released from presynaptic nerve terminals in the central nervous system (CNS) and spreads excitation by binding to and activating postsynaptic iGluRs. Of the potential glutamate targets, tetrameric AMPA receptors mediate fast, transient CNS signaling. Each of the four AMPA subunits in the receptor channel complex is capable of binding glutamate at its ligand-binding domains and transmitting the energy of activation to the pore domain. Homotetrameric AMPA receptor channels open in a stepwise manner, consistent with independent activation of individual subunits, and they exhibit complex kinetic behavior that manifests as temporal shifts between four different conductance levels. Here, we investigate how two AMPA receptor-selective noncompetitive antagonists, GYKI-52466 and GYKI-53655, disrupt the intrinsic step-like gating patterns of maximally activated homotetrameric GluA3 receptors using single-channel recordings from cell-attached patches. Interactions of these 2,3-benzodiazepines with residues in the boundary between the extracellular linkers and transmembrane helical domains reorganize the gating behavior of channels. Low concentrations of modulators stabilize open and closed states to different degrees and coordinate the activation of subunits so that channels open directly from closed to higher conductance levels. Using kinetic and structural models, we provide insight into how the altered gating patterns might arise from molecular contacts within the extracellular linker-channel boundary. Our results suggest that this region may be a tunable locus for AMPA receptor channel gating.

Introduction

The most prominent features of homotetrameric α-amino-3-hydroxy-5-methyl-4-isoxazolepropionic acid (AMPA) receptor channel behavior are the independent activations of individual subunits that manifest as step-like transitions between closed and four open conductance levels, and wanderlust kinetics (Silberberg et al., 1996), previously described in cell-attached patch studies of modal gating behavior (Poon et al., 2010, 2011, 2016). Recent structural studies have correlated open, closed, and desensitized states to conformational changes in the tetrameric AMPA receptor channel complex (Twomey and Sobolevsky, 2018). In addition, probing and modeling AMPA channel gating using receptor-selective noncompetitive antagonists that interact with a key locus in the AMPA receptor channel-gating mechanism is now feasible because of the elucidation of binding sites for three chemically distinct compounds located on individual subunits near the extracellular side of the ion channel domain (Yelshanskaya et al., 2016). Small differences in the molecular contacts made by drugs binding within this region are likely to underlie different functional effects of these drugs.

Previously, the 2,3-benzodiazepines compounds GYKI-52466 (GYKI-52) and GYKI-53655 (GYKI-53) used here were found to potentiate modestly at low concentrations (GYKI-52; Arai, 2001) and inhibit fully at higher concentrations (GYKI-52 and GYKI-53; Ritz et al., 2011; Wang et al., 2014; Wu et al., 2014) AMPA receptor-mediated responses in whole-cell recordings. Both of these drugs suppress seizures in animal models of epilepsy (Donevan et al., 1994; Rogawski, 2011), and GYKI-52 also promotes survival of brain tissue in a hypoxic/ischemic injury model in rats, suggesting a possible prophylactic use of allosteric AMPA antagonists to offset potential post-surgical cognitive decline (Nayak and Kerr, 2013).

The crystal structure of the homotetrameric GluA2 receptor with GYKI-53 bound in the closed channel conformation (Yelshanskaya et al., 2016) showed drug molecules making direct contacts with the preM1 linker and the M1, M3, and M4 helices of each subunit. However, a series of studies investigating the kinetic mechanism of a few 2,3-benzodiazepine compounds in whole-cell recordings provides evidence for binding to open

Department of Molecular Medicine, Cornell University, Ithaca, NY.

*Edward Y. Shi, Christine L. Yuan, and Matthew T. Sipple contributed equally. ; Correspondence to Linda M. Nowak: lmn1@cornell.edu; Robert E. Oswald: reo1@cornell.edu; Edward Y. Shi is currently an MD student at the State University of New York Downstate Medical Center, Brooklyn, NY. Matthew T. Sipple is currently an MD/PhD student at the University of Rochester School of Medicine and Dentistry, Rochester, NY. Christine L. Yuan is currently an MD student at the University of Texas Southwestern Medical School, Dallas, TX.

as well as closed states of the channel (Ritz et al., 2011; Wang et al., 2014; Wu et al., 2014). A clue as to how the GYKI compounds effect their changes in channel gating is found in two recent cryo-EM studies that provide the first high-resolution views of the L2 to preM1 and L1 to M4 linkers in a fully (Chen et al., 2017; Twomey et al., 2017) or partially (Chen et al., 2017; Twomey et al., 2017) open and a fully closed AMPA receptor channel. These cryo-EM structures show that, in the newly resolved fully or partially open conformation of an AMPA receptor, twofold symmetry is found at the linker-channel junction, while four-fold symmetry is observed in the closed channel conformation (Chen et al., 2017; Twomey et al., 2017). Combining this information with that from the crystal structures with GYKI-53 bound suggests that the four modulator sites available in the closed conformation of AMPA receptor channels are reduced to two sites in the open channel complex.

Here, we propose an equilibrium binding model for GYKI-52 and GYKI-53 that is consistent with the open and closed structures and our electrophysiological analysis of whole-cell concentration–effect data and single-channel recordings. Extensive analysis of control recordings of fully glutamate bound subunits under nondesensitizing, activated state conditions yielded additional insights into AMPA channel-gating behavior in cell-attached patches. Long recordings were broken into segments and sorted to reflect kinetic behavior that yielded different patterns of open level occupancy. Except for highly active control channels with very low closed probability (P_C >10%) that required a different approach, we applied methods used in earlier studies (Poon et al., 2010, 2011). Functional differences observed in the presence of either GYKI-52 or GYKI-53 were analyzed in the context of the AMPA receptor's kinetic variability. At 5–20 µM GYKI-52, where only slight inhibition was observed in whole-cell recordings, single-channel gating was remarkably cooperative as the channels opened to, and closed from, only one of four conductance levels in different patches. GYKI-53 (10 µM) altered the AMPA receptor gating mechanism less dramatically, but also produced openings to higher conductance levels from the closed level. The mechanism of action of these modulators on single-channel gating is discussed in the context of open and closed channel structures.

Materials and methods
Cell culture
Human embryonic kidney (HEK) 293 cells were transfected with GluA3$_i$-G (flip; Sommer et al., 1990) and G in R/G editing site (Lomeli et al., 1994) using a mammalian vector that expresses resistance to blasticidin (Thermo Fisher Scientific), and stable cell lines were established as described previously (Holley et al., 2012). GluA3$_i$-G expressing cells were cultured (37°C, 5% CO_2) in Dulbecco's Modified Eagle's Medium supplemented with 1 µg/ml blasticidin, 1% penicillin/streptomycin, and 10% FBS.

Electrophysiology
Whole-cell patch clamp
Recordings were performed on cells 30–48 h after passage using an Axon Instruments 200B amplifier (Molecular Devices) as in Holley et al. (2012). Thin-wall borosilicate glass pipettes (1.5–4 MΩ; Sutter Instrument) were filled with (in mM) 135 CsF, 5 CsCl, 10 EGTA/1 CaCl$_2$, and 10 HEPES/6 CsOH, pH 7.35. The external bath solution contained (in mM) 150 NaCl, 2.8 KCl, 1.0 CaCl$_2$, and 10 HEPES/NaOH, pH 7.4. Cells were exposed to 5 mM L-glutamate (Sigma-Aldrich), with and without inhibitors present to obtain concentration–effect data over a range of inhibitor concentrations (30 nM to 200 µM), depending upon drug potency. Stock solutions of GYKI-52 and GYKI-53–HCl (2–10 mM; Abcam) were prepared in deionized distilled water or ethanol. Cyclothiazide (CTZ) stock solutions (50 or 100 mM; Abcam) were prepared in DMSO, and aliquots were stored at –20°C for up to 6 wk. All recording solutions contained 100–300 µM CTZ. Cells were held at –60 mV, and solutions were applied to cells by sequential superfusion of control (± modulator) followed by glutamate (5 mM) or glutamate + modulator solutions. Data were filtered (5 kHz; Axopatch amplifier; Molecular Devices) and digitized at 20 kHz using QuB software (Nicolai and Sachs, 2013) and a data acquisition/SCXI switching system (DAX M series 622x; National Instruments Corp.).

Single channel recording
Cell lines with –100 to –250 pA responses to 10 mM glutamate + CTZ in whole-cell recordings were used. Cell-attached patches were formed on cells bathed in Dulbecco's phosphate buffered saline (Invitrogen) with 1.0 mM MgCl$_2$ added. Pipettes (15–20 MΩ; standard-wall borosilicate glass with filament; Sutter Instrument) were pulled, fire polished, and filled with pipette solution that contained (in mM) 150 NaCl, 10 HEPES/6 NaOH, pH 7.5, 2 KCl, 0.25 CaCl$_2$, and 5 L-glutamate-Na$^+$ with CTZ (100–150 µM), either with or without an inhibitor present. Inhibitor stock solutions were serially diluted in pipette solution. Pipette solutions were made every 1.5 h to maintain the CTZ concentration.

Single-channel currents were amplified using an EPC-7 (100 mV/pA; HEKA Instruments). Recordings were filtered using the amplifier filter (10 kHz) plus an external 10-kHz filter (8-pole Bessel; Frequency Devices) in series to an effective low-pass filter of 7.07 kHz (–3 db) before digitization (20 kHz) using QuB software. Single-channel current recordings (5–60 min) were obtained in cell-attached mode. Pipette holding potentials (V_p) of 120 or 130 mV were used to improve detection of transitions between conductance levels.

Analysis of single-channel data
Properties of channels obtained during stable recordings were assessed using QuB software at 30- to 60-s intervals to confirm that equilibrium conditions were met and that the patch was not damaged during the recording, which is usually seen as a decrease in amplitude for all step levels as cell resting potential decreases. Only cell-attached patch recordings that showed no evidence of a second channel present were used to investigate gating properties. While the first minute of a recording generally revealed whether multiple channels were present in the absence of inhibitors, the entire recording was scrutinized carefully for large-amplitude openings that would signal the presence of a second channel in the patch when inhibitors were present. Patches

Shi et al.
Antagonist-induced cooperative AMPA receptor gating

Journal of General Physiology 157
https://doi.org/10.1085/jgp.201812209

containing one channel were analyzed with QuB software as described in Poon et al. (2010, 2016).

All recordings were idealized using the segmental k-means (SKM) algorithm (Qin and Li, 2004), as described previously (Poon et al., 2010), with a 100-µs sample interval. SKM idealization was performed using a linear model with one closed and four open levels (C, O_1, O_2, O_3, and O_4) that were selected with noise to generate idealized events. This process yielded amplitude probability density functions (pdfs) that were used to define occupancy per level (C and O_1–O_4), and the tables of idealized events used to enumerate the transitions between adjacent and nonadjacent conductance levels used to construct T-matrix event tables (software developed in the laboratory) as follows. The percentage of transitions reported in the cells of a T-matrix was calculated by dividing the number of transitions in any given cell by the total number of transitions detected in the whole record. The effect of dead time on detection of adjacent versus nonadjacent transitions in the T-matrix analysis of channels recorded under control conditions (5 mM glutamate, 150 µM CTZ, 7-kHz filter, and 20-kHz sampling) was examined by systematically changing the sampling interval for the idealization from 50 to 400 µs (in 50-µs increments). The percentage of nonadjacent transitions increased with the increased dead time (e.g., from 1.1% to 8.8% for control data). T-matrix data were helpful in generating reaction mechanisms for channels exposed to GYKI-53 with two caveats: they are based on the number of conductance levels selected for the idealization, and although very brief transitions were included due to the 100-µs sampling parameter, it is necessary to recognize they are below the dead time applied to kinetic modeling.

Idealized events were subjected to maximum interval likelihood (MIL) analysis (Qin et al., 1996) initiated using a 300-µs dead time, and transition rates in the model were set to 100 s^{-1} for the first MIL run. States were added one at a time to closed and open classes, with the number of exponential components in the dwell-time histograms dictating the number of states added per conductance class. Data were reanalyzed using MIL to remodel the data as each new state was added until the overall global model met two main criteria: fits to the closed and open dwell-time histograms improved visibly, and the log-likelihood (LL)/event unit increased by at least 0.01. If including another state increased the LL/event statistic produced by the MIL algorithm, and one or more of the rates were unrealistically large or near zero, the additional state was deleted, and the data were refit using the previous model. When a near-final model was obtained, each of the rates was systematically perturbed to address the potential problem of local minima (Poon et al., 2016). Final models for control data contained two to four closed states and two to three states per open level. These branched models were linear with the additional states within each of the conductance levels branching off the main C, O_1, O_2, O_3, O_4 reaction scheme. As reported by Poon et al. (2010, 2011), we observed that building cyclical models that included loops connecting nonadjacent conductance levels failed to improve the LL statistics, or did not visibly improve dwell-time fits, and/or introduced unrealistic transition rates. Although loop models are not reported here for control data, they were applied to data with

GYKI-53 present, and detailed balance constraints were applied to rates within loops.

### Occupancy analysis of AMPA receptor gating

Poon et al. (2010) observed that kinetic parameters shifted frequently during most cell-attached patch recordings, and described this behavior as *modal*. They used the critical closed time (t_{crit}) method to identify segments containing groups of openings separated by long closures. Segments with long closures and few openings were discarded, and those remaining were sorted using the X-means algorithm as described by Pelleg and Moore (Pelleg, D., and A.W. Moore. 2000. ICML Proceedings of the 17th International Conference on Machine Learning) into kinetic patterns based on the probability the channel was fully closed (P_C) as reviewed in Poon et al. (2016). Five kinetic modes were identified over a range of glutamate concentrations (50 µM to 5 mM) in the presence of CTZ (Poon et al., 2010); openings to a fourth conductance level recorded were too infrequent to be identified without ambiguity in recordings with a lower signal-to-noise ratio.

In the present study, all recordings were made in the presence of 5 mM glutamate, and the t_{crit} method was applied to the control recordings that showed $P_C > 0.10$ and to recordings obtained with inhibitors present. However, ~40% of control channels exposed to 5 mM glutamate were so active that their closed state occupancy was <10%. These channels were also more likely to open to a fourth conductance level (O_4) with 3–30% of the area of the amplitude pdf in O_4 compared with previous recordings with 1–3% O_4 in 1 mM glutamate (Poon et al., 2016). Given that the channel was more likely fully open than closed, fluctuating kinetics of highly active single channels were investigated by dividing records into 5-s segments, idealizing them using the SKM algorithm with one closed and four open levels as described above, then using the X-means algorithm to sort the segments based on the fully open (P_{O4}) occupancy. The resulting categories were referred to as occupancy patterns. Two to three activity patterns were obtained for control channels that opened mainly to O_3 and O_4 levels, and one or two patterns were obtained for channels that opened mainly to O_1 and O_2 levels. Control and GYKI single-channel data are presented here in the context of open conductance patterns.

Energy landscapes

Energy landscape plots provide an illustration of the energy of each state relative to the others, with the C_a closed state (adjacent to the first open conductance level) defined as the zero-energy level in each plot. The plots were constructed as follows: the equilibrium constant (K_{eq}) for each state in the reaction mechanism was calculated as the ratio of the forward to backward rates for each transition, and the ΔG_0 was defined as $-RT\ln K_{eq}$ to determine the relative energy level. The heights of barriers between transitions were scaled to the log of the forward rate. Barriers between the states represent the energy required to make transitions between the different open levels and adjacent states. The main barriers between C_c, C_b, C_a, O_{1a}, O_{2a}, O_{3a}, and O_{4a}, representing opening and closing of subunits, are connected by a black line, while transitions between adjacent states within each open conductance level (the branches) are presented in a color and offset from the
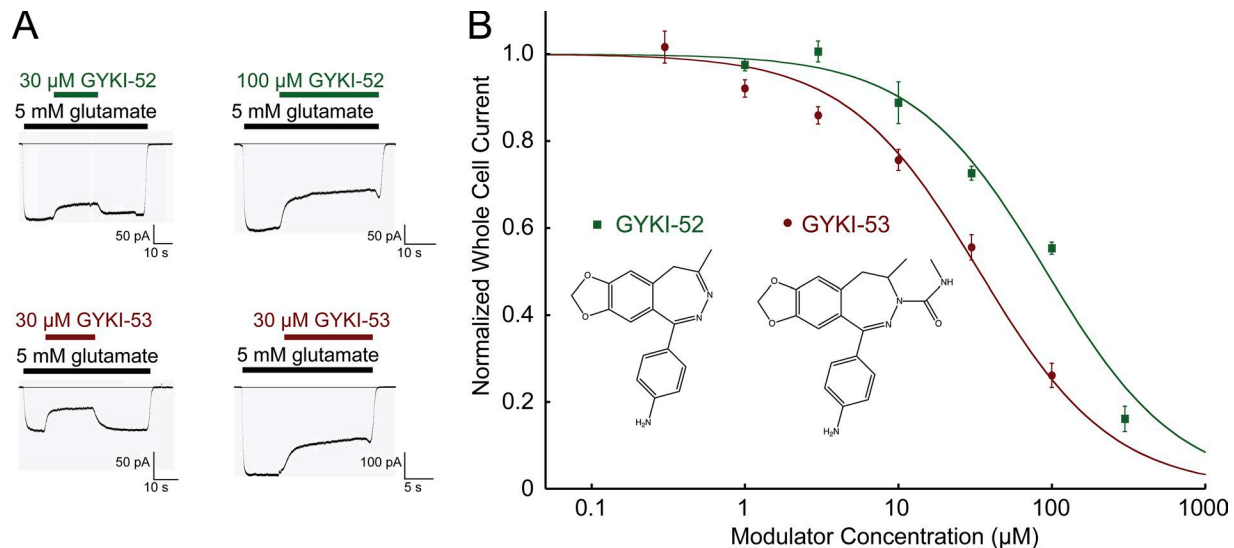
Figure 1. **Whole-cell responses, concentration–effect curves, and structures of GYKI-52 and GYKI-53. (A)** Examples of responses to 30 and 100 µM GYKI-52 (top), and 30 µM GYKI-53 (bottom) recorded from different cells (V_h = –60 mV) demonstrate inhibition using different protocols. Control and drug solutions contained CTZ. **(B)** Whole-cell responses to inhibitors were normalized to currents in 5 mM glutamate alone applied to all cells to obtain concentration–inhibition curves. Individual cells were exposed (up to three times) to one, two, or three different concentrations of GYKI-52 (30 cells) or GYKI-53 (23 cells). Symbols/error bars represent the mean ± SEM for 3–10 cells. Inset: Chemical structures of the modulators (GYKI 52466: CAS RN 102771–26-6, GYKI 53655: CAS RN 143692–18-6) show that these molecules are similar except GYKI-53 has a 3-methylcarbamyl moiety.

main set of energy barriers. States with the greatest thermal stability are negative relative to the C_a state. Energy landscapes not only allow visualization of differences in kinetic patterns, but also show the barrier height between transitions, thereby providing information that cannot be gleaned simply from the inspection of the rates within the reaction mechanism or by calculation of equilibrium constants. Thus, energy landscapes provide a simplified picture for comparison between control channel kinetic behaviors and those observed with a modulator present.

Online supplemental material

The Supplemental text is a description of how the equilibrium binding model was formulated. Tables S1, S3, and S5 summarize time constants obtained from fitting dwell-time histograms to control, GYKI-52, and GYKI-53 data and Tables S2, S4, and S6 summarize equilibrium constant values obtained for control, GYKI-52, and GYKI-53 data from the QuB fits of the reaction schemes used to model transitions between states for single-channel data.
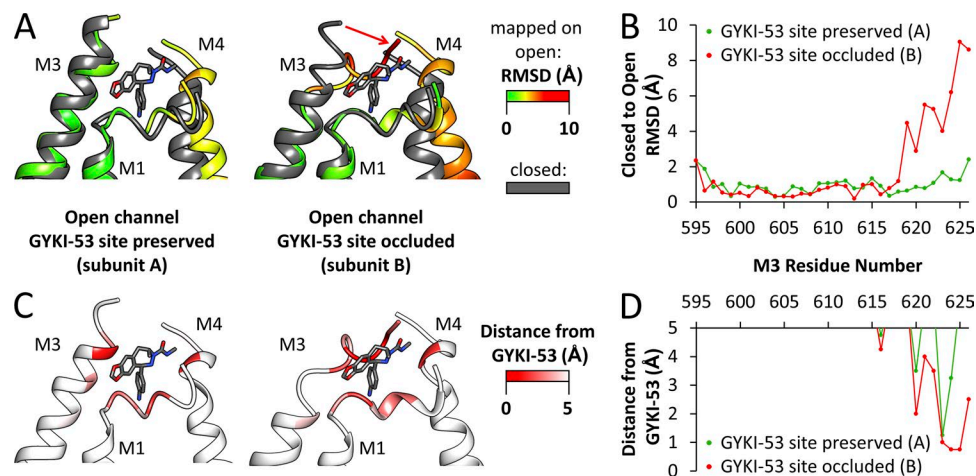
Figure 2. **Analysis of AMPA receptor open state–GYKI-53 interactions. (A)** Individual subunits of the open structure (PDB ID: 5WEO; Twomey et al., 2017) of the AMPA receptor ion channel domain were aligned with the best fit GYKI-53 bound closed structure (gray, PDB ID: 5L1H; Yelshanskaya et al., 2016) using UCSF-Chimera (Pettersen et al., 2004). Open-state channel subunit A (left) maintains a GYKI-53 binding site, while in channel subunit B (right), the GYKI-53 binding site is occluded by the shift in M3 linker (red arrow). **(B)** The RMSD between Cα atoms in closed and open structures is mapped onto the open-state channel structures and plotted for both subunit A (preserved) and B (occluded). **(C)** The distance between GYKI-53 and the open-state channel subunit A (left, preserved) and subunit B (right, occluded) is mapped onto the open-state structure. The shortest nonhydrogen atom–atom distances between a residue and GYKI-53 are displayed for positions with distances <5 Å. **(D)** The GYKI-53 to M3 residue distance is plotted for open-state subunits A (preserved) and B (occluded). In the open-state subunit B (occluded), atoms from Phe623, Leu624, and Thr625 encroach on the GYKI-53 binding site (<1 Å from atoms in GYKI-53).

Shi et al.
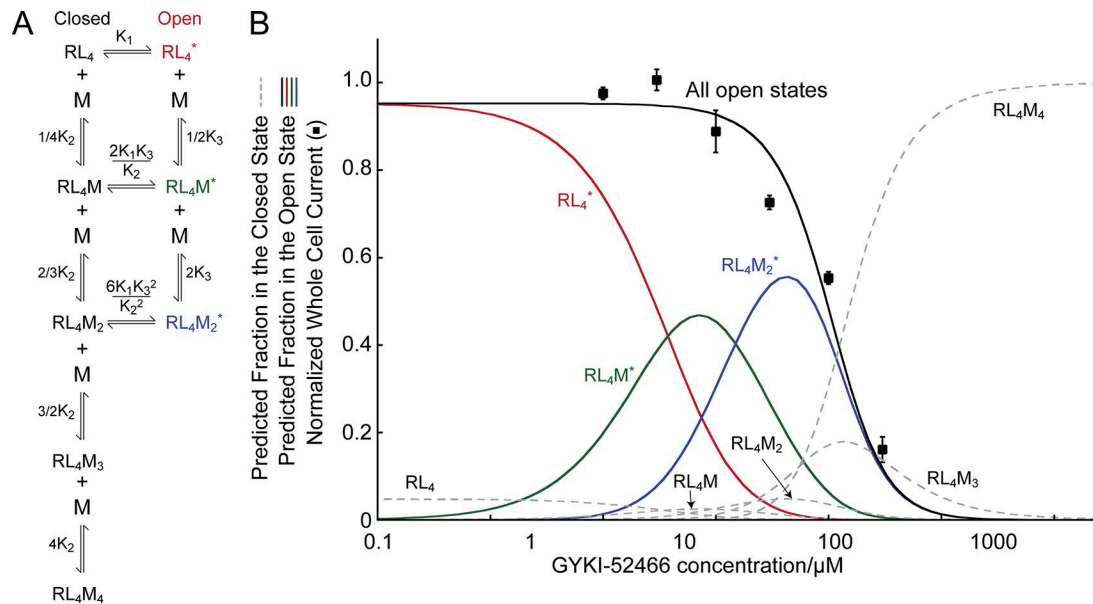Antagonist-induced cooperative AMPA receptor gating

Figure 3. **Equilibrium binding reaction scheme for the allosteric modulator based on closed and open structures of an AMPA channel with GYKI-53 bound. (A)** A reaction scheme for the effects of modulators in whole-cell recordings based on assumed interactions with four sites in the closed and two sites in the open conformations when the LBD is fully occupied by glutamate and CTZ. **(B)** The fit of the model to GYKI-52 concentration–effect data is presented with the predicted normalized whole-cell current resulting from open channels with 0 (red), 1 (green), and 2 molecules (blue) of GYKI-52 bound. The fraction of each closed state is shown as gray dashed lines. The best fit of the equilibrium constants to the data are as follows: $K_1 = 0.05$, $K_2 = 14.5$ μM, and $K_3 = 7.5$ μM. Additional details are in the Supplemental text.

Results

Inhibition of whole-cell responses by GYKI drugs

Whole-cell recordings were performed to obtain the concentration–effect relationships in Fig. 1. Responses to increasing concentrations of GYKI-52 and GYKI-53 were normalized to the control (glutamate plus CTZ) responses in each recording, and data were fit assuming a simple model of inhibition. GYKI-53 was about threefold more potent than GYKI-52 with IC_{50} values of 34 ± 3.6 μM for GYKI-53 and 92 ± 13 μM for GYKI-52.

Previous whole-cell studies suggested that GYKI compounds interact with open as well as closed conformations of AMPA receptor channels (Ritz et al., 2011; Wang et al., 2014; Wu et al., 2014). In addition, GYKI-52 is sometimes reported to potentiate agonist responses at low concentrations (Arai, 2001; Wang et al., 2014; Wu et al., 2014). Analysis of recent cryo-EM structures of GluA2 in its open and closed conformations (Chen et al., 2017; Twomey et al., 2017) along with the crystal structures of GluA2 with GYKI-53 bound (Yelshanskaya et al., 2016) shown in Fig. 2 support the hypothesis that GYKI molecules can interact with open as well as closed channel conformations when the receptor is fully agonist bound and the noncompetitive antagonist concentration is low. The open channel structure of an AMPA receptor is particularly important for understanding the mechanisms of GYKI modulator effects, as it indicates that in the transition to the fully open channel, rearrangement of the linker between the M3 helix and the ligand-binding domain (LBD) occludes two of the four modulator binding sites (Fig. 2). Thus, there are four available sites in the closed conformation, but only two modulator binding sites are available in the fully open state. In the closed conformation, GYKI-53 (and by analogy GYKI-52) binds to all four subunits at the top of the ion channel domain. GYKI-52 is

related to GYKI-53, but it is a smaller, fully planar molecule that lacks the methylcarbamyl group at position 3 (Fig. 1). Based on the similar structures of the two molecules, the binding position of GYKI-52 is likely to be similar to GYKI-53. The movement of the M3 linker into the binding position occupied by the core benzodiazepine ring shared by GYKI-52 and GYKI-53 in the closed conformation would possibly prevent a GYKI-bound closed subunit from opening.

An equilibrium model for modulator binding and inhibition is shown in Fig. 3. The model is based on the structural data constraints for modulator molecule interactions within a tetrameric AMPA receptor. It assumes there is no cooperativity for modulator binding and that LBDs in all four subunits are bound by agonist (Fig. 3 A). The fitting of the GYKI-52 whole-cell concentration–effect data by this model is illustrated in Fig. 3 B. At higher modulator concentrations, consistent with full inhibition, GYKI compounds would be bound to four closed subunits. An essential feature of this model, however, is that at low modulator concentrations where only a small amount of inhibition is observed, the modulator can bind to sites available on open subunits. Importantly, in the 10–20 μM range, all of the channels are likely to have GYKI-52 (or GYKI-53) bound to subunits in open conformations. This model was employed as a framework for interpreting the single-channel data.

Maximally activated AMPA receptor channels in the absence of modulators
Four active subunits per channel

Homomeric GluA3$_i$-G AMPA receptor channels were recorded in cell-attached patches using 5 mM L-glutamate and 150–200 μM CTZ, pH 7.5, to activate maximally the receptors in this study.
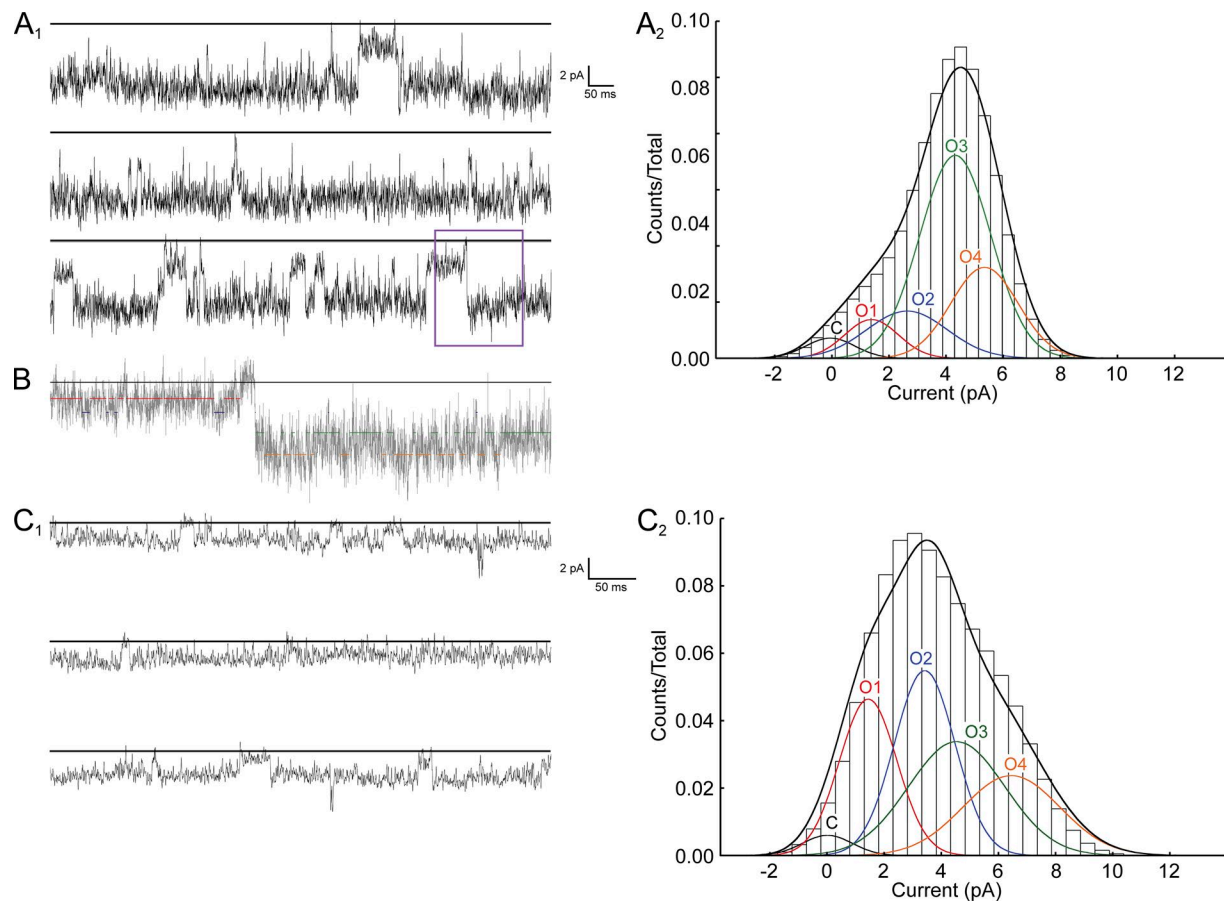
Figure 4. Single-channel recordings of a GluA3 homomeric channel exposed to 5 mM L-glutamate and 150 µM CTZ that was closed (black line) <5% of the time. (A₁) The channel mainly opened to the O_3 and O_4 levels in this 3-s continuous data trace, while in C, it frequently was open to the O_1 and O_2 levels (1-kHz filter/20-kHz sampling). **(B)** A portion of A_1 (box) has color-coded lines that show C, O_1, O_2, O_3, and O_4 levels (7-kHz filter/20-kHz sampling) detected during idealization using the SKM algorithm. Amplitude pdf histograms (A_2 and C_2) of single-channel currents recorded during two 10-min segments of a 30-min recording were each fit with the sum of five Gaussian functions representing the fractional occupancy (area) for each conductance level (P_C, P_{O1}, P_{O2}, P_{O3}, and P_{O4}) versus the total area. Mean amplitudes of three combined 10-min segments were (±SEM) 0.053 pA ± 0.09, 1.5 (± 0.12), 3.0 (± 0.36), 4.6 (± 0.18), and 5.9 (± 0.55) pA for C, O_1, O_2, O_3, and O_4, respectively. Baseline recording noise (measured in the closed channel) was 0.92 ± 0.023 pA (for recording acquired at V_p 120 mV, 7-kHz filter/20-kHz sampling).

Control recordings analyzed in this section are later compared with channels exposed to negative allosteric modulators in cell-attached patch pipettes containing the same concentrations of L-glutamate and CTZ. The normally low expression level of GluA3i-G homomeric channels, coupled with selection of stably transfected cell lines that had maximum whole-cell responses of ∼200 pA, resulted in patches containing only one channel per patch ∼40% of the time. Analysis of long records (5–60 min) in the absence of desensitization confirmed the presence of only one channel and allowed fluctuations in kinetic behavior to be detected and analyzed.

Single-channel amplitude changed in steps between adjacent levels to four different open-channel amplitudes in all control patches. Temporal variability in the number of simultaneously active subunits was consistent with modal gating and was manifested by shifts in mean occupancy levels O_2, O_3, and O_4 (Fig. 4). Step-like amplitude transitions are consistent with activation of four individually opening subunits. Open level slope conductance values from five single-channel, cell-attached patches recorded between V_p 80 and 160 mV were 10 ± 5.1, 23 ± 1.9, 33 ± 3.4, and

47 ± 1.5 pS (mean ± SD). Although all of the control channels exhibited four open levels, the probability of populating any given open level varied between patches. Channels that opened to O_3 and O_4 levels more than 20% of the time are referred to as high-activity channels (P_{O3-4} = 0.37 ± 0.14, n = 3), and those that opened to O_3 and O_4 levels less than 20% of the time as low-activity channels with mean P_{O1-2} 0.36 ± 0.10 (n = 5). Closed probability was greater in low-activity channels (P_C 0.17 ± 0.12, n = 5) compared with high-activity channels (P_C 0.031 ± 0.025, n = 3).

Correlating kinetics and occupancy in maximally activated channels

Long recordings typically included periods during which lower conductance levels were occupied and other periods during which intermediate or higher conductance levels predominated, consistent with previously reported modal gating. Maximally activated GluA3 homomeric channels typically remained in a particular mode/pattern for longer than seen in lower concentrations of glutamate (Poon et al., 2010). The high-activity channel exemplified in Fig. 4 shifted its kinetic behavior throughout
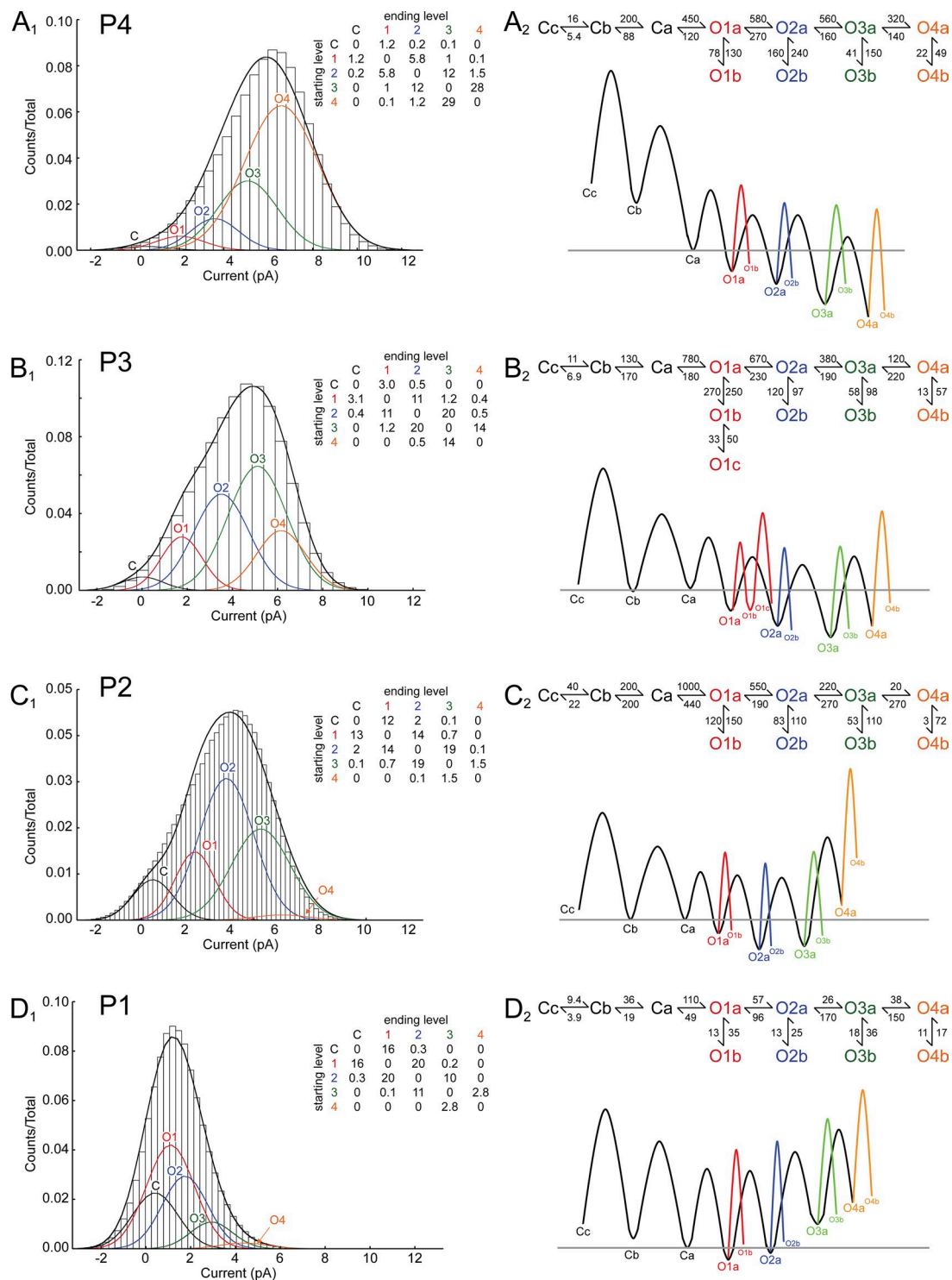
Shi et al.
Antagonist-induced cooperative AMPA receptor gating

Figure 5. **Subunits of GluA3 homomeric channels open independently, displaying high- and low-activity patterns.** A five-component model (C, O_1, O_2, O_3, and O_4) was used for SKM idealization producing amplitude pdf histograms where the component with the largest fractional area in the pdf ordained it activity pattern assignment, to P4 (high P_{O4}), to P3 (high P_{O3}), and to P2, (high P_{O2}). **(A_1–C_1)** Amplitude histograms were obtained from a high-activity channel; **(D_1)** the histogram in was obtained from a lower activity channel. Transition matrix tables for A_1 through D_1 show that conductance changes occur mainly between adjacent conductance levels. Kinetic modeling produced a set of linear–branched reaction schemes. Energy landscapes show that transitions between conductance levels are favored compared with transitions to second (or third) states within each level. **(A_2–D_2)** The LL statistics for fitting the 11 or 12 state linear-branched models in were 3.72, 3.63, 3.85, and 2.82 LL/events, respectively. LL statistics for all control data are summarized in Table 2 by patterns P1–P4. The dwell-time histograms fit with two or three exponential components are in Fig. 6. Time constant values (with areas) and the mean LL/event statistics for open and closed states of all GluA3 homomeric channels recorded without inhibitors are provided in Table S1.

Table 1. Fractional occupancy and transition data summary of control recordings after segment sorting

Occupancy pattern	C	O_1	O_2	O_3	O_4	Adjacent transitions	Total no. of events
P4 $n = 3$	0.016 ± 0.010	0.104 ± 0.079	0.111 ± 0.066	0.330 ± 0.079	**0.440 ± 0.158**	97.1 ± 2.3%	71,134
P3 $n = 2$	0.044 ± 0.019	0.126 ± 0.010	0.264 ± 0.039	**0.472 ± 0.102**	0.095 ± 0.093	92.7 ± 0.3%	315,560
P2 $n = 3$	0.064 ± 0.041	0.237 ± 0.188	**0.448 ± 0.114**	0.232 ± 0.122	0.009 ± 0.007	96.3 ± 2.4%	357,792
P1 $n = 4$	0.192 ± 0.127	**0.476 ± 0.048**	0.268 ± 0.121	0.044 ± 0.008	0.015 ± 0.004	99.5 ± 0.5%	117,552

Single-channel events recorded in eight cell-attached patches resulted in 12 files with a sufficient number of events for fitting multistate kinetic models. Patterns P1–P4 each represent the highest fractional occupancy in each of the O_1–O_4 levels. Values for open levels with the greatest fractional area are bolded. Transitions to adjacent conductance levels were >90% for all four occupancy patterns. Mean values ± SD represent the sum of events from all patches (n) in that pattern.

the 30-min recording. Each of the four activity patterns (P1–P4) in Fig. 5 correlates with a predominant open level (O_1, O_2, O_3, or O_4). Three occupancy patterns were generally observed for high-activity channels, and two patterns were typical of low-activity channels; each of the four open levels was observed in all four patterns.

An amplitude histogram, transition matrix, kinetic model, and energy landscape plot for each pattern (P1–P4) are shown in Fig. 5. The channel amplitude stepped to adjacent levels among the five conductance levels (C, O_1, to O_2, to O_3, and O_4) in all occupancy patterns (P1–P4), consistent with the hypothesis that individual subunits of AMPA receptor channels gate independently. A summary of the fractional occupancies of the five conductance levels for each of patterns P1–P4 is provided in Table 1.

Kinetic models were linear (transitions existed only between adjacent conductance levels with no loops), but with branches to one, two, and three different kinetic states within a conductance level (Fig. 5). Dwell-time histograms are shown in Fig. 6, with time constant (mean ± SD) values for control recordings summarized in Table S1.

The slowest forward rates were associated with P1 behavior, and the fastest ones were associated with P4 behavior. Equilibrium constants calculated (forward rate divided by reverse rate) for each transition in control data parsed into patterns are provided in Table S2.

For each model in Fig. 5, energy landscapes show the relative energies for transitions (barriers) between states (wells) required for the shifts in conductance levels from "closed" to fully open (continuous black line), and the transitions between states within each open level (color matched to conductance). Overall, open states are favored over closed states in 5 mM glutamate with CTZ present, even when a channel opened mainly to level O_1 as in Fig. 5 D. The heights of the series of barriers from closed to the O_4 level were lower for P4 than those for other patterns, and the barriers for an open subunit to closed were higher than for an additional subunit to open, consistent with the faster forward rates and a greater probability for each of the four subunits to enter its open conformation. P1 and P2 energy landscapes (Fig. 5, D_2 and C_2) showed that while transitions from closed to open are favored, openings to higher conductance levels were not, consistent with fewer simultaneously open subunits.

GYKI-52 stabilizes open channels

GYKI-52 is a smaller molecule and a weaker antagonist than GYKI-53. Small increases in whole-cell current were seen with 3 and 10 µM GYKI-52 in only a few cells exposed to 5 mM glutamate (data not shown). Given the variability of effects reported in whole-cell recording with low concentrations of GYKI-52, we elected to investigate how this drug affects single-channel behavior at low concentrations where its inhibitory effects would be emerging but minimal.
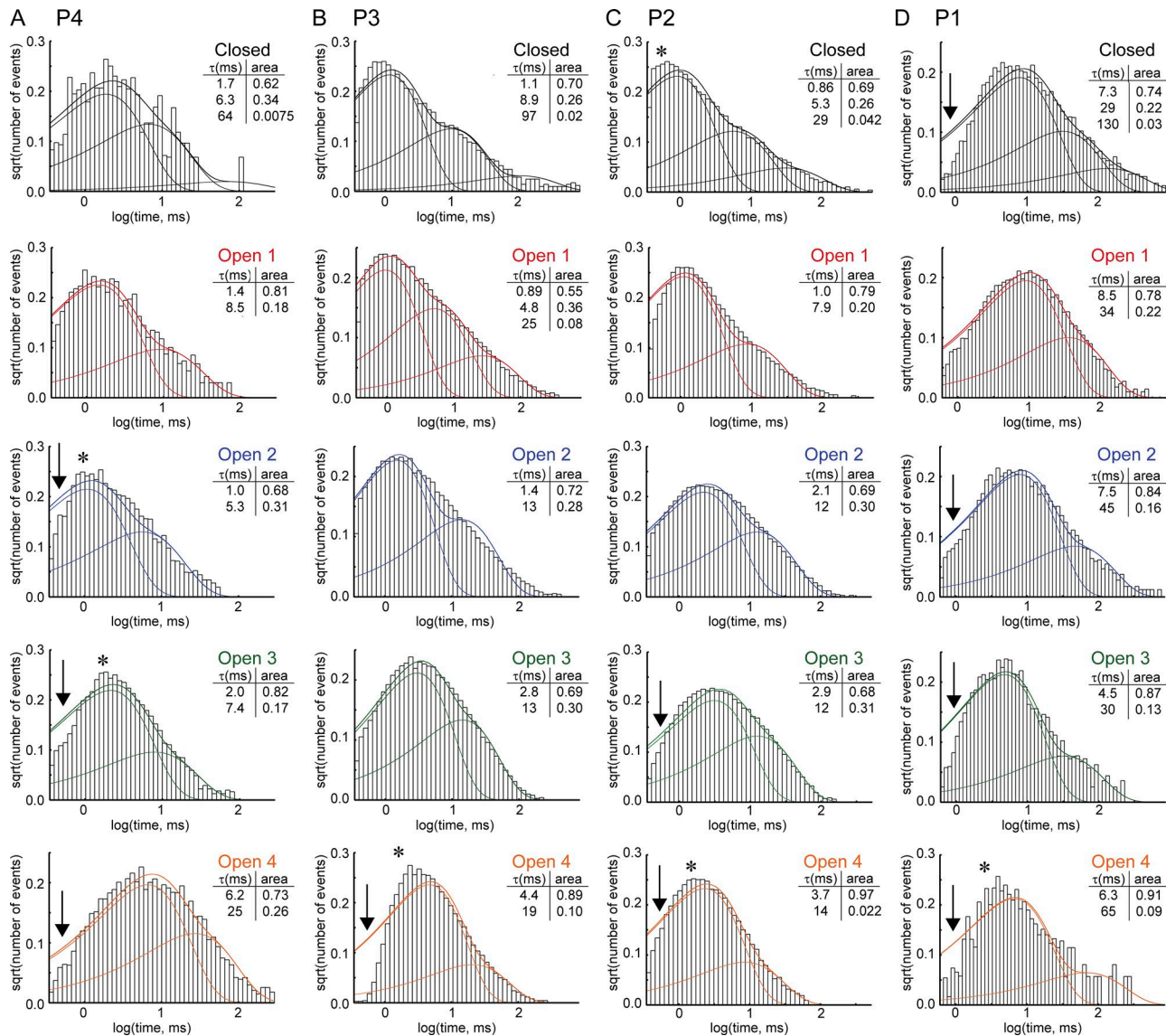
The effects of GYKI-52 (10 and 20 µM) on single-channel behavior were striking in that, instead of opening to four different levels, channels opened to only one level in six of eight 10–30 min recordings. Thus, the primary pattern of channel activity was closed–open (C–O), in which the channel opened to level O_x directly from closed (where x = 1, 2, 3, or 4). Transitions to adjacent levels for the duration of the recordings were rare and data were modeled using a linear C–O reaction mechanism. Compared with control records, GYKI-52 increased closed probabilities in all but those with the P1 occupancy pattern, which appeared unchanged from low-activity channels in control.

Six of eight recordings exhibiting the C–O gating pattern had transitions mainly between nonadjacent conductance levels (Table 2). The two other recordings exhibiting a C–O gating pattern had transitions only between C and O_1. In the P3b record, where there were transitions to more than one level, the channel opened mainly to O_3, with transitions out of O_3 to C > O_4 > O_2. In the P2b record, the channel opened mainly from closed to O_2 with ~37% of transitions between O_2 and O_3.

Channels that opened to either O_3 or O_4 in GYKI-52 did so with higher probability than high-activity channels in controls (P_{O3-4} 0.59 ± 0.093 versus 0.37 ± 0.14, respectively), and they also had higher P_C in GYKI-52 than high-activity controls (P_C 0.38 ± 0.094 versus 0.031 ± 0.025, respectively). For channels opening mainly to O_1 and O_2 levels in GYKI-52, P_C was similar to controls (0.19 ± 0.13 versus 0.17 ± 0.12), but P_{O1-2} was higher than in control recordings (0.76 ± 0.20 versus 0.36 ± 0.10). Thus, the increased P_C associated with inhibition observed in higher-activity channels is offset at least partially by increasing P_O in low-activity channels.

Examples of channels opening directly to the O_4 level are shown in Fig. 7 A and to the O_2 level are shown in Fig. 7 B. Energy landscape plots in GYKI-52 (Fig. 7, A_3 and B_3) show that the brief closed state (C_a) is less stable than the longer closed states.

Shi et al.
Antagonist-induced cooperative AMPA receptor gating

Journal of General Physiology 163
https://doi.org/10.1085/jgp.201812209

Figure 6. **Dwell-time histograms for C, O_1, O_2, O_3, and O_4 conductance levels are shown with two or three exponential fits for each conductance level for patterns P1–P4. (A)** The closed dwell-time of P4 contained too few events due to low P_C (0.010) to be well fit. **(B–D)** Closed dwell-time histograms of P1–P3 were well fit by the sum of three exponential components. **(A–C)** Open dwell-times of P2–P4 were well fit by the sum of two or three exponential components. **(D)** The O_4 level of P1 contained too few events to be fit well. Time constants (τ) and areas are shown with the histogram for each of the states in the models provided in Fig. 5. The QuB fitting algorithm corrected the data for missing brief events (arrows) due to the 300-μs dead time. The excess numbers of brief events in some dwell-time histograms (e.g., see asterisk in closed, O_1, and O_4 histograms) represent promotion of a brief event to the next higher bin (Colquhoun and Sigworth, 1995). The y axes of the histograms represent the square root of the number of events divided by the total number of events in the plot, the x axis is time (in milliseconds) on a $\log_{10}$ scale, and the time constant for each state is at the maximum number of events for each exponential component (Sigworth and Sine, 1987).

Open states are more stable than any of the closed states. The difference in the open dwell-time distributions with GYKI-52 was striking compared with control data, as there is a much larger fraction of long openings in the presence of GYKI-52 (Figs. 6 and 8). Closed time distributions in GYKI-52 show that the number of longer and intermediate closures increased compared with control recordings (Figs. 6 and 8). Control and GYKI-52 time constant data are summarized in Tables S1 and S3. Equilibrium constant values are provided in Tables S2 and S4.

Given the complex step transition patterns seen in the absence of modulators, the appearance of an AMPA channel open-

ing directly from closed directly to O_2, O_3, or especially O_4 for 10s of minutes was remarkable, and suggests that GYKI-52 induces cooperativity in channel opening and closing. This cooperativity may at very low concentrations lead to extremely modest potentiation of whole-cell currents, but the overall effect on whole-cell current is an inhibition due to the fact that the closed state is also significantly stabilized. Possible mechanisms underlying the emergence of this behavior are presented in the discussion. Fractional occupancy data for channels exposed to GYKI-52 is summarized in Table 2, and average time constant values are provided in Table S3.
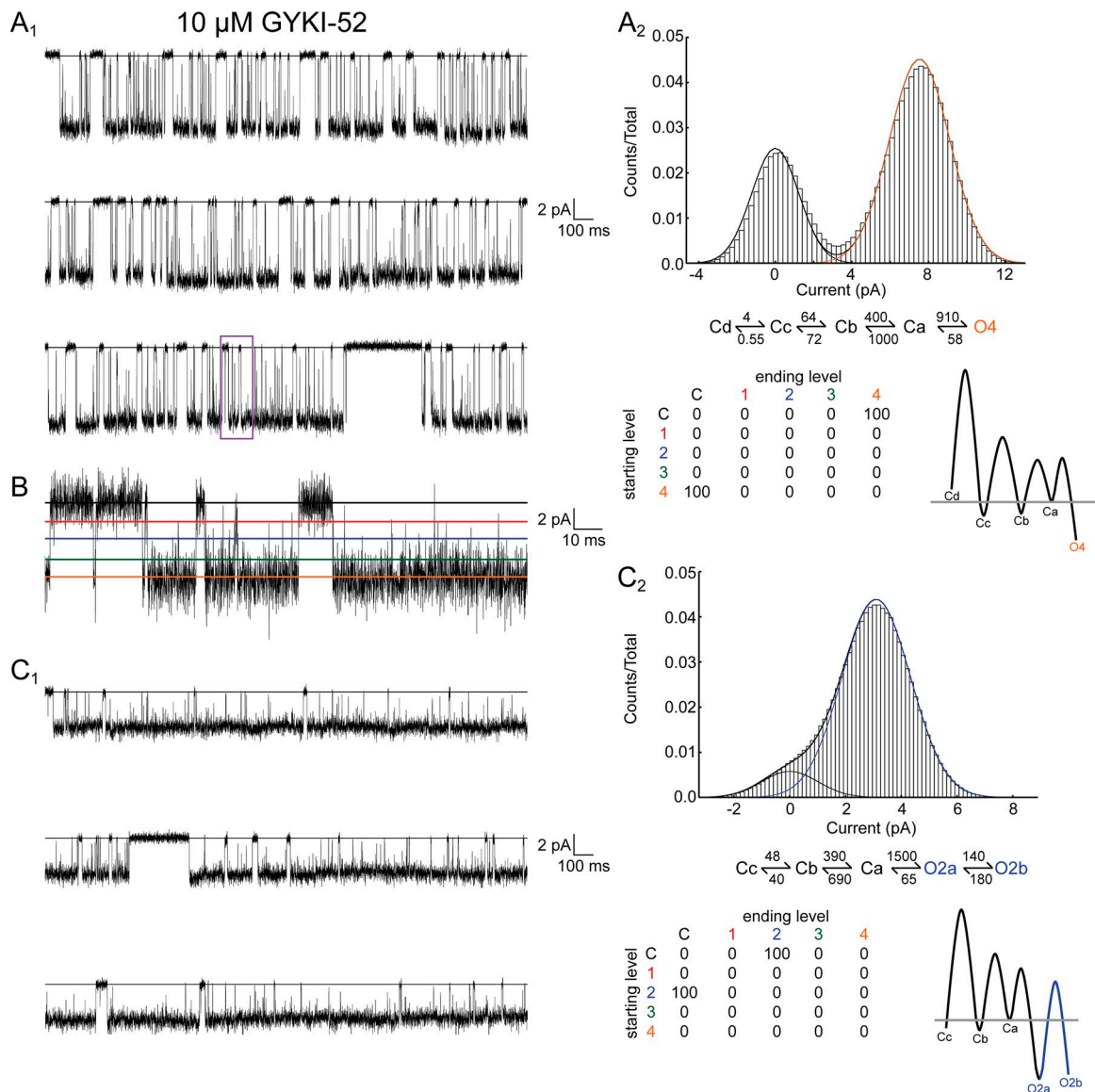
Figure 7. **GYKI-52 induced gating changes in GluA3 channels for all occupancy levels. (A₁)** The channel in this recording opened from closed to level O_4 in the presence of 10 µM GYKI-52 in the pipette illustrated with 1-kHz filter/20-kHz sampling. **(A₂)** Data were idealized using a C–O model and fit by four closed (C_{a-d}) and one open (O_4) state (Fig. 8 A). O_4 was the most stable state in the energy landscape with C_b and C_c states energetically favored over the C_a state. **(B)** A portion of A_1 (box) has color-coded lines to indicate expected C, O_1, O_2, O_3, and O_4 levels (7-kHz filter/20-kHz sampling). **(C₁)** Another channel opened from closed to O_2 with 10 µM GYKI-52 in the pipette illustrated with 1-kHz filter/20-kHz sampling. **(C₂)** The amplitude pdf shows that the channel is mostly open and the reaction mechanism shows transitions between C_a and O_2. Data were fit with three closed (C_{a-c}) and two open ($O_{2a,b}$) states (Fig. 8 B). O_{2a} and O_{2b} were the most stable states in the energy landscape, and the lowest energy barrier was for the transition from C_a to O_{2a}. The barrier from O_{2a} to O_{2b} was lower than the one to C_a, while the barrier from O_{2a} to C_a was more than twice as high, consistent with the greater stability of the longer open state. Among closed states, C_b and C_c were more stable than C_a and C_d, which is in contrast to control P1–P3 behavior, where the C_a states have lower or similar energy compared with other closed states.

GYKI-53 modifies GluA3 channel-gating kinetics

GYKI-53 (10 µM) is a more potent inhibitor than 10 µM GYKI-52 in whole-cell recordings, and its ability to coordinate single AMPA channel gating was less obvious in raw data traces. Two types of channel activity were observed in separate patches with GYKI-53: channels that opened mainly to the O_3 and O_4 levels (fit by loop models) and channels that opened mainly to the O_1 and O_2 levels (fit by linear–branched models).

Consistent with inhibition of whole-cell currents, P_C increased for recordings of single channels exposed to 10 µM GYKI-53.

Compared with control recordings under similar conditions, P_C was 0.45 ± 0.24 for the two channels in GYKI-53 that preferentially opened to O_3 and O_4, and it was 0.23 ± 0.17 (n = 5) for channels opening mainly to O_1 and O_2 versus control values of the P2 (0.031 ± 0.025; n = 3) and P1 (0.17 ± 0.12; n = 5) groups, respectively. Table 3 reports fractional occupancy in different conductance levels, including P_C, in the presence of GYKI-53 following t_{crit} sorting, which removes the longer closures between bursts of openings.

Gating patterns for channels opening to higher conductances in GYKI-53 differed from channels under control conditions and

Shi et al.
Antagonist-induced cooperative AMPA receptor gating

Table 2. Fractional occupancy and transition values by O_X levels for recordings of channels in the presence of glutamate and GYKI-52

Occupancy pattern	C	O_1	O_2	O_3	O_4	Adjacent transitions	Total no. of events
P4 $n = 1$	0.306	–	–	–	0.694	0%	42,537
P3a O_3 $n = 1$	0.484	–	–	0.516	–	0%	78,537
P3b $n = 1$	0.342	–	0.098	0.418	0.142	51.4%	22,594
P2a O_2 $n = 2$	0.245 ± 0.207	–	0.755 ± 0.207	–	–	0%	21,355
P2b $n = 1$	0.238	–	0.486	0.275	–	36.9%	16,681
P1 $n = 2$	0.108 ± 0.037	0.893 ± 0.037	–	–	–	100%	46,234

Data are from eight recordings that were not segmented or sorted. Six channels opened to one level, and two others (P3b, P2b) opened to one or two additional levels. Entries without ± SD represent single patches.

those exposed to GYKI-52. The channel in Fig. 9 A was exposed to 10 µM GYKI-53. It opened to all four open-conductance levels, but mostly to level O_3. The occupancies of closed and O_3 levels were 36% and 48%, respectively, while the combined occupancy of O_1, O_2, and O_4 was only 16%. Unlike control records, a significant fraction of transitions were to nonadjacent conductance levels (see T-matrix in Fig. 9 A), producing a two-loop reaction mechanism.

Transition matrices in P1- and P2-like patterns in GYKI-53 resembled those in the control data with >90% of transitions to adjacent conductance levels (compare Tables 1 and 3) producing a linear–branched reaction mechanism (Fig. 9 B).

Evidence for increased stability of closed states in the P3/P4-like patterns can be gleaned from the dwell-time histogram in Fig. 10 A_1, and the mean time constant and equilibrium constant data summarized in Tables S5 and S6. Examination of Fig. 10, A_1 and A_4 shows the increased areas of longer closed and open states compared to, for example, dwell-time distributions for any of the controls (P1–P4) in Fig. 6. In addition, comparison of the equilibrium constant values in the control and with GYKI-53, from which the energy levels in the energy landscapes would have been derived (Tables S2 and S6), shows higher K_{eq} values for the transitions between longer closed states than for the C_a to O_{Xa} opening transitions. P1/P2-like occupancy behavior was associated with stabilization of longer open states (Fig. 10 B_3), but less dramatically than in GYKI-52 (Fig. 8 B_2).

Comparing effects of GYKI compounds across modes
Fig. 11 summarizes control and modulator fractional occupancies in C, O_1, O_2, O_3, and O_4 using data from Tables 1, 2, and 3. Channels that frequented O_3 and/or O_4 conductance levels in GYKI-52 and GYKI-53 differed from control recordings in that P_C increased and openings to O_1 and O_2 were infrequent (Figs. 5, A and B; 7 A; and 9 A). Both GYKI-52 and GYKI-53 appeared to potentiate openings to the O_2 level, compared with control P2 behavior. GYKI-52, but not GYKI-53, increased O_1 level openings compared with control. Overall, taking into account the differences in open and closed dwell times (Figs. 6, 8, and 11; and Tables S2, S4, and S6), it appears both GYKI compounds stabilize closed conformations of AMPA receptor channels, but GYKI-52 stabilizes open conformations better than GYKI-53.

In contrast to control recordings where channels opened and closed >90% of the time to an adjacent conductance level in P1–P4, the GYKI drugs introduced coupling between subunits,

seemingly in a pattern-dependent way. Both GYKI compounds strongly coordinated openings in the P3/P4 patterns. GYKI-53 modulated channels in the P3- and P4-like patterns frequently opening and closing to nonadjacent levels, and most nonadjacent transitions skipped one level as if pairs of subunits were coupled. Channels modulated by GYKI-52 rarely transitioned between adjacent levels, except, of course, for those in the P1 group that opened between C and the O_1 level. Closed-channel occupancy increased in the P3- and P4-like patterns in GYKI-52 and GYKI-53, and closed states were stabilized along with the preferred open state. GYKI-53 and GYKI-52 appeared to increase O_2 occupancy in the P2 patterns without much increase in P_C. Overall, these patterns are consistent with the hypothesis, provided in Fig. 12 and elaborated more fully in the discussion, that the GYKI compounds may be functionally coupling pairs of subunits through binding to one subunit while interacting with the M3 helix of an adjacent subunit through a cross-linking effect of the GYKI 4-aminophenyl group.

Discussion
Selecting recording conditions
Nearly all structural studies of AMPA receptors use the GluA2 subunit (Pøhlsgaard et al., 2011; Twomey and Sobolevsky, 2018), which is nearly identical in primary structure to GluA3 subunits (Boulter et al., 1990). We have used homomeric GluA3$_i$G receptors because the low expression of stably transfected HEK293 cells allows for long and stable recordings of single-channel behavior (Poon et al., 2010, 2011, 2016).

It is known that AMPA receptors share a common set of structural motifs (Wo and Oswald, 1995) with each of the four subunits within the holoreceptor contributing an extracellular amino-terminal domain, an LBD, a transmembrane/ion-channel domain, and an intracellular C-terminal domain. The receptors assemble as a dimer of dimers, and agonist molecules bind between lobes 1 and 2 (L1, L2) of each of the bilobate LBDs in the tetrameric complex. Agonist binding causes a transition from an open LBD to a closed-cleft conformation that initiates subunit activation and/or desensitization (Armstrong et al., 1998; Armstrong and Gouaux, 2000; Sun et al., 2002; Sobolevsky et al., 2009). The back-to-back orientation of adjacent L1/L1 subunits within the LBD forms a

Occupancy pattern	C	O_1	O_2	O_3	O_4	Adjacent transitions	Total no. of events
P4 $n = 2$	0.423 ± 0.058	0.040 ± 0.013	0.021 ± 0.018	0.093 ± 0.007	**0.425 ± 0.061**	69.6 ± 4.3%	41,564
P3 $n = 3$	0.417 ± 0.140	0.032 ± 0.045	0.043 ± 0.041	**0.468 ± 0.072**	0.041 ± 0.022	60.0 ± 18.1%	123,644
P2 $n = 2$	0.079 ± 0.000	0.091 ± 0.010	**0.740 ± 0.005**	0.092 ± 0.005	–	91.7 ± 3.3%	292,596
P1 $n = 2$	0.298 ± 0.130	**0.437 ± 0.063**	0.242 ± 0.102	0.024 ± 0.024	–	99.3 ± 1.0%	32,546

Data from seven patches subjected to t_{crit} segmentation yielded nine files that contained sufficient numbers of events for kinetic modeling. Values for open levels with the greatest fractional areas are bolded.

dimer interface in closed receptor channels. As the agonist binding cleft closes around an agonist, strain on the LBD dimer interface causes the dimer to break apart and leads to desensitization of the receptor (Sun et al., 2002; Gonzalez et al., 2010). A potent positive modulator, CTZ, which binds to and stabilizes the dimer interface (Ptak et al., 2014), suppresses desensitization and increases the open channel lifetime (Mitchell and Fleck, 2007). CTZ was used here as described previously (Poon et al., 2010), in order to establish a set of stable recording conditions for maximally activating AMPA receptor channels in the control recordings as well as channels with GYKI compounds bound. Studying desensitizing AMPA receptors in cell-attached patches, which include very long closed periods and very few full channel openings, would have made determination of the number of channels in a patch difficult and essentially impossible in the presence of inhibitors.

Previously, low amplitude events were observed at lower agonist concentrations, and the frequency of higher amplitude events increased in a concentration-dependent manner, suggesting that agonists bind to and activate subunits individually in the AMPA receptor channel complex (Rosenmund et al., 1998; Smith and Howe, 2000). Four open conductance levels were reported for channels recorded in outside-out patches (Prieto and Wollmuth, 2010; Zhang et al., 2017), but Poon et al. (2011) observed three open conductance levels for partial agonists (chloro-, fluoro- and nitro-willardiines) and also for glutamate in cell-attached patch recordings. Here, we increased the pipette holding potential from 100 and 110 mV to 120 and 130 mV, which allowed observation

of an additional, fourth open level. The increase in membrane potential across the patch provided better separation of the step changes in amplitude, and using 5 mM here, rather than 1 mM glutamate (Poon et al., 2016), increased the number and duration of O_4 level openings in cell-attached patches.

Channel gating in the absence of drug
Variability of gating patterns in fully activated GluA3$_i$-G channels
AMPA receptor channels exhibit shifting kinetic patterns during long cell-attached patch recordings. Modal gating is a recognized feature of single-channel kinetic studies of AMPA receptor channels, having been demonstrated in cell-attached patch (Poon et al., 2010, 2011, 2016) and outside-out patch recordings (Prieto and Wollmuth, 2010) in the absence of auxiliary proteins, and in recent studies where GluA2 and TARP γ2 were coexpressed (Zhang et al., 2014). In the latter, the presence of γ2 subunits increased open probability and modal gating in the absence and presence of CTZ. Here, we report four different gating patterns with different probabilities of each of four open conductance levels.

Independent subunit opening is a hallmark of AMPA receptor channels
A few studies of homomeric AMPA channels expressed in HEK cells recorded in outside-out patches have suggested that there may be some degree of cooperativity in AMPA channel gating (Rosenmund et al., 1998), particularly at negative membrane potentials (Prieto and Wollmuth, 2010). Coordination of subunit
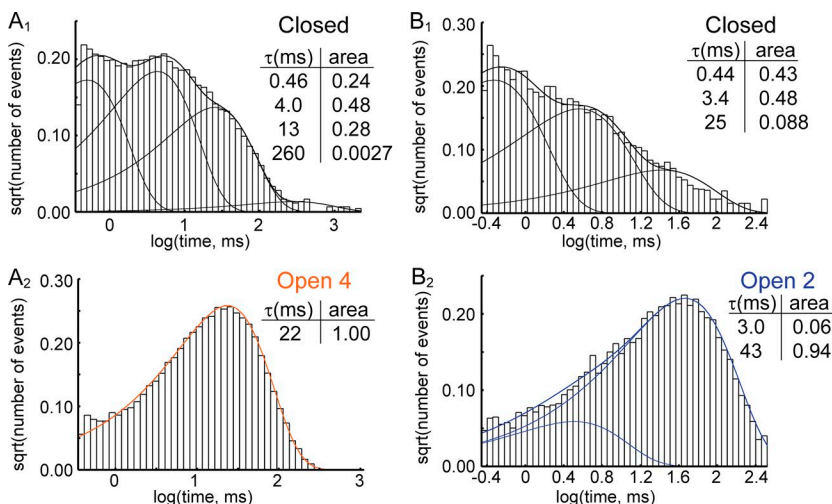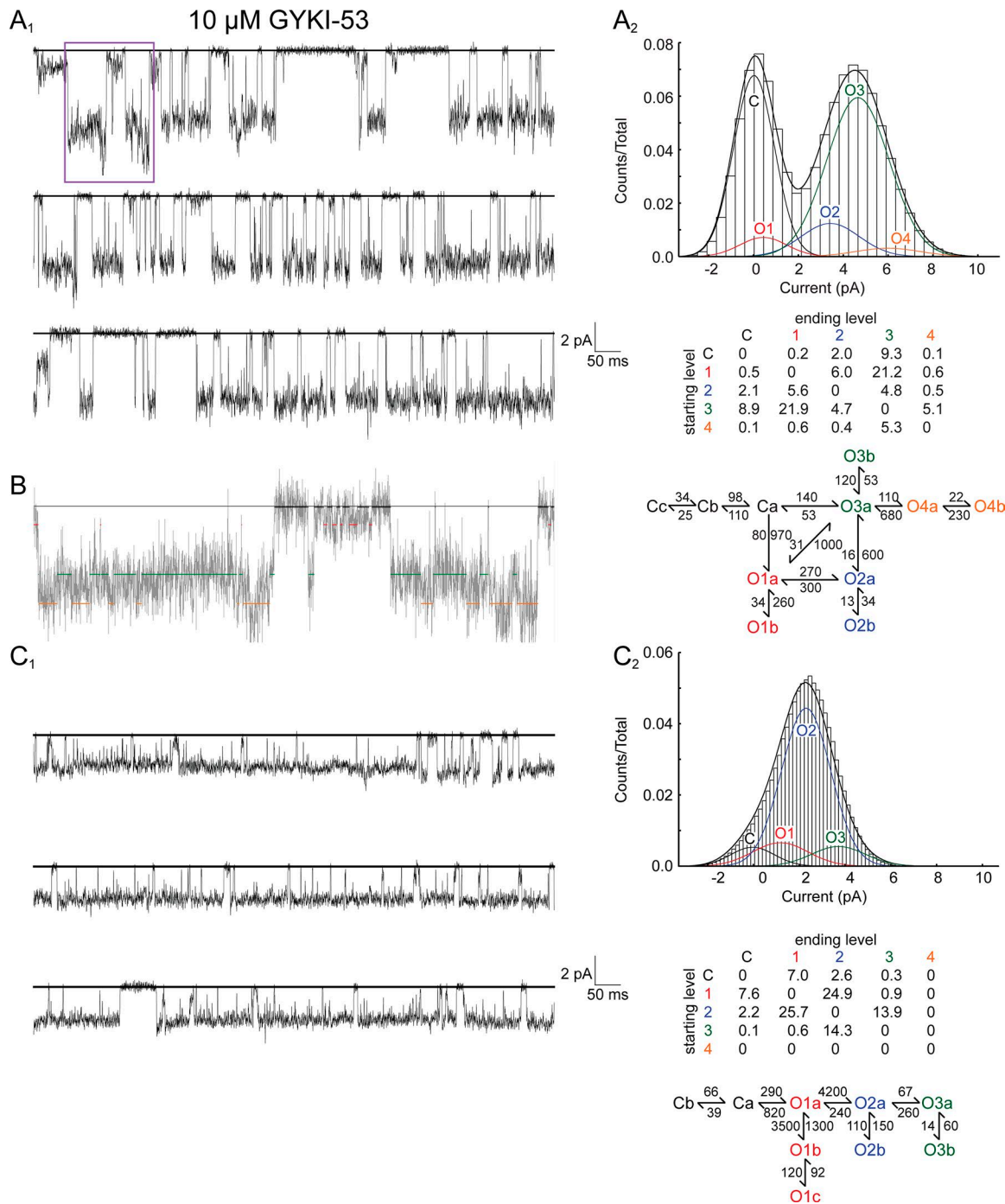

Figure 8. **Closed and open events distributions for channels exposed to GYKI-52 reflect altered gating patterns. (A$_1$ and A$_2$)** Closed and open time distributions for the channel in Fig. 7 A. The relative area for the C$_a$, C$_b$, and C$_c$ states in GYKI-52 are similar. Stabilization of the O$_{4b}$ state is also evident in the open time distribution (A$_2$) where nearly all events were long duration, to the extent that a single time constant fit most of the data without including the small number of brief events. **(B$_1$ and B$_2$)** Closed and open dwell-time distributions are shown for the channel in Fig. 7 B that opened to level O$_2$. The area of the C$_b$ state is increased and the open channel stability is evident in the large area subsumed by O$_{2b}$. Compare these histograms to control ones in Fig. 6 and dwell-time values with areas in Tables S1, S3, and S5.

A_1 10 µM GYKI-53

2 pA
50 ms

A_2

	ending level				
starting level	C	1	2	3	4
C	0	0.2	2.0	9.3	0.1
1	0.5	0	6.0	21.2	0.6
2	2.1	5.6	0	4.8	0.5
3	8.9	21.9	4.7	0	5.1
4	0.1	0.6	0.4	5.3	0

B

C_1

2 pA
50 ms

C_2

	ending level				
starting level	C	1	2	3	4
C	0	7.0	2.6	0.3	0
1	7.6	0	24.9	0.9	0
2	2.2	25.7	0	13.9	0
3	0.1	0.6	14.3	0	0
4	0	0	0	0	0

Figure 9. Gating effects of GYKI-53 differed between P3/P4-like and P1/P2-like occupancy patterns. (A_1) Three seconds of continuous recording from a cell-attached patch exposed to 10 µM GYKI-53 shows the majority of openings are to O_3, although events in O_1, O_2, and O_4 are observed. **(A_2)** The amplitude pdf for this recording shows a channel with probability of being open mainly to O_3 (0.48) or closed (0.36) with less than 10% of openings to any of the other levels (O_1, 0.044; O_2, 0.093; and O_4, 0.026). The T-matrix table indicates a complex array of transitions between both nonadjacent and adjacent states. Data were fit with a two-loop reaction mechanism (LL/event of 3.60; 98,027 events; Fig. 10 A). **(B)** A portion of A_1 (box) has color-coded lines that show idealized C, O_1, O_2, O_3, and O_4 levels (7-kHz filter/20-kHz sampling) detected using the SKM algorithm. **(C_1)** Three seconds of continuous recording for a channel opening mainly to O_2 (pre-t_{crit} analysis occupancy values were 0.188, 0.148, 0.585, and 0.078 for C, O_1, O_2, and O_3, respectively). **(C_2)** Following t_{crit}-based sorting, the channel mainly occupied level O_2 (0.709), with smaller fractions of C, O_1, and O_3. No O_4 openings were detected, and 6% of transitions were to nonadjacent conductance levels. The linear–branched model represented in C_2 had an LL/event of 3.29 (67,583 events; Fig. 10 B).

opening has not been observed in cell-attached patch recordings in HEK cells using glutamate or partial agonists (Poon et al., 2010, 2011), where it is possible to record thousands of openings from a single homomeric GluA3$_i$-G channel. Here, we confirm our previ-

ous finding of independent gating in control cell-attached patches with both very low- and very high-activity channels recorded with maximally activated GluA3 receptor channels. For channels in P2–P4, the total number of transitions observed between nonadjacent
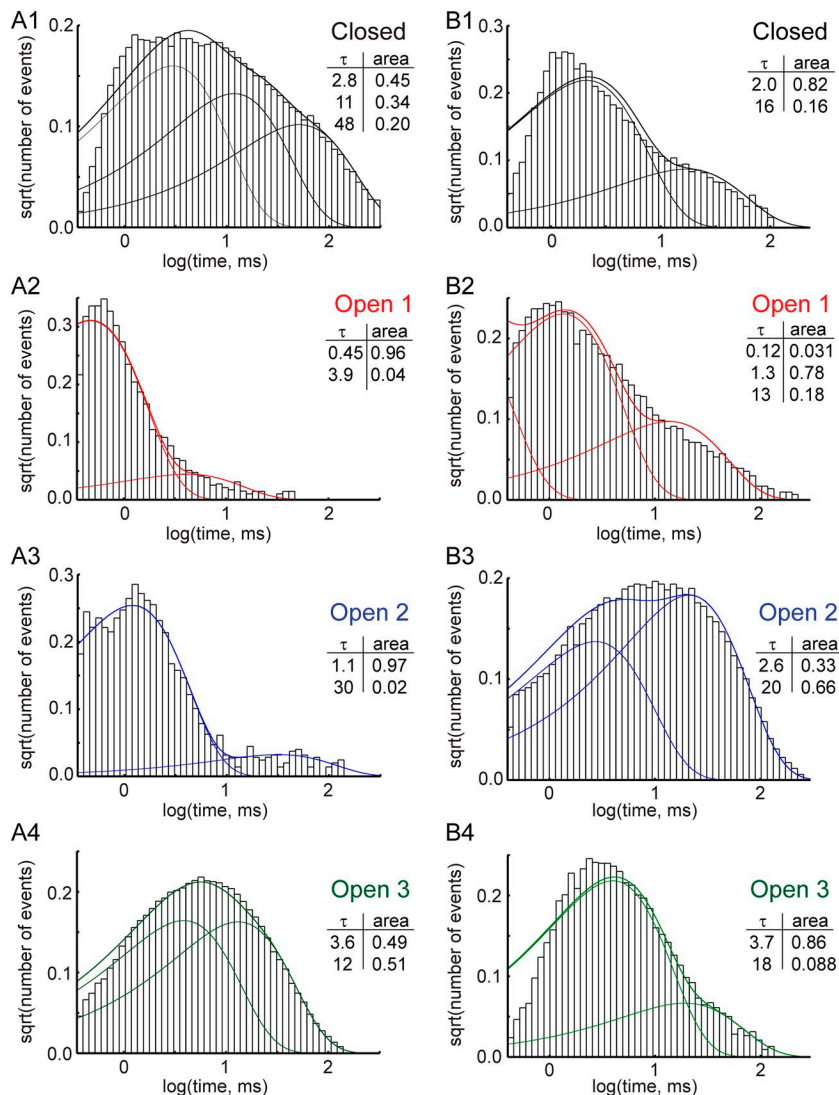
Figure 10. **Closed and open events distributions for channels exposed to GYKI-53 differ from those in GYKI-52. (A1–A4)** Closed and open time distributions for the channel in Fig. 9 A. The relative area for the C_a, C_b, and C_c states (A1) are similar. Stabilization of the O_{4b} state is evident in the open time distribution (A2), where nearly all events fall into the longer duration group. **(B1–B4)** Closed and open dwell-time distributions are shown for the channel in Fig. 9 B that opened to level O_2. The area of the C_b state is increased and the open channel stability is evident by the large area subsumed by O_{2b}. Compare these histograms to control ones in Fig. 6 and dwell-time values in Tables S1, S3, and S5.

conductance levels varied between 1 and 10% (Table 1). Because of the inevitable limit on temporal resolution imposed by filtering data during acquisition, near simultaneous transitions from, for example, O_1 to O_2 and O_2 to O_3, could be misinterpreted as a single, nonadjacent transition from O_1 to O_3. To determine if this effect contributes to the small number of nonadjacent transitions observed, the possibility was tested post hoc by varying the dead time imposed by the filtering and sampling frequencies during modeling. This analysis showed that an increased number of nonadjacent transitions were observed with increasing dead time (see Materials and methods). Thus, within the constraints imposed by the original filtering and sampling parameters in our recordings, it appears that individual subunits of homomeric GluA3$_i$G receptors expressed in HEK 293 cells are opening independently.

iGluR gating is controlled at the extracellular linker–membrane helix junction

Through functional and structural analysis of the effects of mutations at the junction between the transmembrane helices and the flexible extracellular linkers to the LBDs, this region has emerged as a focal point for understanding similarities and differences be-

tween iGluR receptors in health and disease. In particular, the A/T point mutation associated with the *Lurcher* gating phenotype in mice (Zuo et al., 1997) is located in the highly conserved SYTANL AAF motif. Both NMDA (Blanke and VanDongen, 2008; Talukder et al., 2010, 2011; Murthy et al., 2012; Alsaloum et al., 2016) and AMPA receptors (Zuo et al., 1997; Taverna et al., 2000; Klein and Howe, 2004; Zhang et al., 2017) bearing this point mutation have altered gating patterns. Based on systematic mutations and computer simulations, the concept of a gating collar at the level of the extracellular linkers has been proposed for AMPA receptors (Yelshanskaya et al., 2017). This region also provides a receptor-specific target area for pharmacological agents (Yelshanskaya et al., 2016; Perszyk et al., 2018). Combining insights gained from these studies with precise localization of GYKI-53 binding sites within this region, the model presented in Fig. 3 established the basis for understanding dynamic aspects of AMPA receptor channel behavior.

Noncompetitive antagonist effects on fully activated GluA3$_i$-G channels

Two prototype anticonvulsant drugs (GYKI-52 and GYKI-53) are noncompetitive inhibitors of AMPA receptor activation (Hibi et
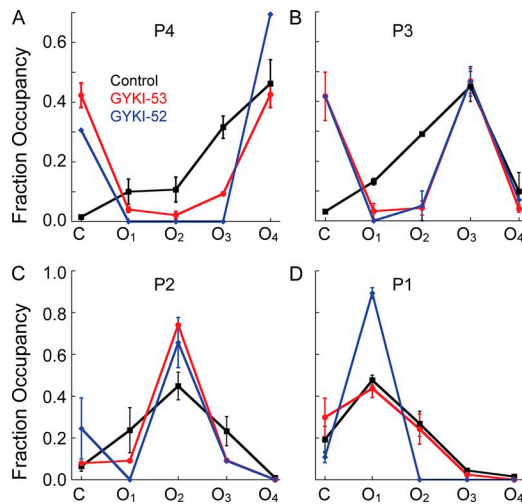
Figure 11. **Summary of the effects of GYKI drugs on gating modes.** Fractional occupancy in C, O_1, O_2, O_3, and O_4 are plotted for GYKI-52 and GYKI-53 compared with control for each of the four modes. **(A and B)** In P3 (B) and P4 (A), P_C increased consistent with inhibition, and there is an apparent coordination of subunits to produce openings to higher conductance levels. **(C and D)** GYKI-53 appeared to potentiate P1 activity while GYKI-52 potentiated both P1 (D) and P2 (C).

al., 2012; Rogawski and Hanada, 2013; Barygin, 2016). The single-channel studies presented here provide new insights into how these 2,3-benzodiazepine drugs exert inhibitory effects, as well as contribute to our understanding of the mechanism of AMPA receptor channel gating. Some effects on the open state had previously been reported for GYKI compounds (Ritz et al., 2011; Wang et al., 2014; Wu et al., 2014), and our single-channel evidence confirms an interaction with open channel states. In particular, GYKI-52 and GYKI-53 coordinate channel openings such that, instead of independent step-like transitions to four characteristic open levels, they mainly produced concerted openings from closed to one of the higher conductance levels, or, as in the case of GYKI-53, coupling between subunits reflected in direct transitions between O_1 and O_3 open levels. How GYKI-52 and GYKI-53 alter AMPA receptor gating patterns is described below in the context of a model derived from recent structural studies and the equilibrium pharmacological response-based model (Figs. 2 and 3; and Supplemental text).

Inhibition and stabilization by GYKI compounds

The energy barrier between the open states and the C_a state is increased by both GYKI compounds, consistent with inhibition; however, open states as well as closed states were stabilized by the inhibitors. Both drugs induced a large fraction of transitions to nonadjacent levels in the P3- and P4-like activity patterns. An obvious difference between the gating patterns observed with GYKI-53 and GYKI-52 was that with GYKI-52, channels mainly opened to one level throughout the recording, while channels in the presence of GYKI-53 opened to different conductance levels throughout the recordings. Together, these observations support the hypothesis that the GYKI drugs (a) can interact with the open state of the receptor and (b) can functionally couple subunits within the receptor channel complex.
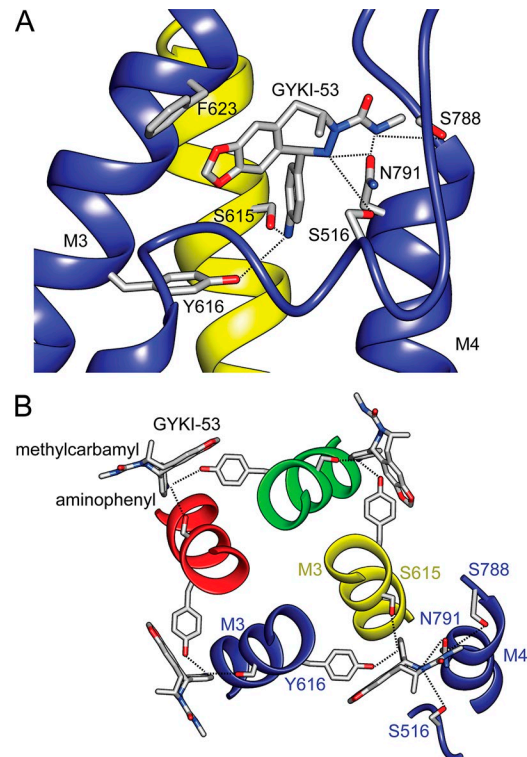

Figure 12. **Two views of GYKI-53 bound to GluA2. (A)** The binding site for GYKI-53 on GluA2 (5L1H; Yelshanskaya et al., 2016) shows the aminophenyl group interacting with S615 of M3 in the D subunit (yellow) and Y616 of M3 in the A subunit (blue). Several interactions with the M4 helix (S788, N791) and preM1 (S516) also contribute to forming the GYKI-53 binding site. Depending on the subunit, rotamers of N791 can interact with either the methylcarbamyl group (shown here) or the aminophenyl group. **(B)** In the extracellular view, intersubunit interactions of GYKI-53 with portions of the M3 helix are shown. Four bound GYKI-53 molecules girdle the closed channel at the extracellular junction with the transmembrane helices. For the A subunit, regions of the M4 helix and preM1 that form the GYKI-53 binding pocket are included.

Single-channel effects of the GYKI compounds in consideration of the structural constraints

While GYKI-53 interacts with Y616 and makes other contacts within a hydrophobic pocket on one subunit, the 4-aminophenyl group of GYKI-53 (present on both GYKI compounds) also interacts with S615 on an adjacent subunit (Fig. 12). Focusing on the Y616/S615 intersubunit interactions of GYKI-53, it is clear that this creates intersubunit constraints, essentially forming a collar of interactions around the outer portion of the channel. With four molecules of GYKI-53 bound, the interactions could prevent the outward movement of M3 and M4 transmembrane helices, thus maintaining the closed state by preventing channel opening. The position of GYKI-53 induces another set of constraints in the gating region through interactions of its 3-methylcarbamyl group with S788 and N791 in M4. When mutated to alanine individually, there are only modest effects on the IC_{50} values of GYKI-53 (Yelshanskaya et al., 2016). The interactions of GYKI-53 with M4 are likely to further stabilize the closed form of the channel. Since GYKI-52 lacks the 3-methylcarbamyl group, and may exhibit weaker interactions with M4, it is possible the GYKI-53/M4 contacts contribute to the greater potency observed with GYKI-53.

The structure of open (Chen et al., 2017; Twomey et al., 2017) or partially open (Chen et al., 2017; Twomey et al., 2017) homomeric GluA2 receptors provides important clues relevant to how these negative modulators may stabilize open states. Whereas the closed channel structure with GYKI-53 bound showed fourfold symmetry in the ion channel and a portion of the linker region that contributes to the GYKI binding site, the linkers in the open channel conformation show a twofold symmetry that begins at the top of the ion channel. In the open conformation, the position of the M3-L2 linkers in the B and D subunits change and prevent the binding of GYKI. Conversely, the binding of GYKI to its site on either of these subunits would prevent the subunits from transitioning to the open conformation (Fig. 2, A and B; and Supplemental text). The M3-L2 linker in the A and C subunits would not prevent modulator binding, but the binding site would be changed somewhat by the outward movement of the M1, M3, and M4 helices and may act as an energy well to stabilize the open conformation. These differences hold important implications for the mechanism of action of the GYKI drugs because the presumption would be that both drugs could bind to all four subunits in the closed conformation, but they may bind to the A and C subunits when they are open, giving rise to a model such as that shown in Fig. 3 A. This model predicts complete inhibition of channel activity at high GYKI concentrations, but stabilization of open states at lower concentrations. If the affinity for the open state were slightly higher than for the closed state, as it may be for GYKI-52, nearly all open channels observed at the low concentrations of GYKI-52 used in the current studies would be bound to the drug (Fig. 3 B). This stabilization would produce an anticonvulsant effect through increased P_C, despite the stabilization of the channel open states, and thus with less overall inhibition at lower concentrations. From a drug design perspective, it provides an interesting alternative mechanism compared with drugs that are potent inhibitors of AMPA-mediated activity as it permits a greater possibility of maintaining a balance between excitation and inhibition.

If binding of a GYKI molecule links together adjacent subunits through the 4-aminophenyl group (Fig. 12), with three or four molecules bound, the linkage would be inhibitory, since it would prevent the outward movement of the helices and channel opening. However, for subunits in their open conformation, only two drug molecules can bind. Thus, when linking drug-bound subunits in an open conformation, there may be synchronized gating with the two adjacent subunits. If GYKI binds to the channel while it is in the closed conformation, the subunits would stay closed. In other words, when the drugs bind to and stabilize the open conformation, they may also prevent adjacent subunits from closing, providing the appearance of transitions between closed and an open conformation that is preferred in the context of the underlying modal activity of the channel. The effect would be most striking for channels operating in P3 and P4, but channels operating in P2 could, under these circumstances, be stabilized in the O_2 level (Fig. 11 C).

Characterization of the single-channel gating in the absence and presence of GYKI-52 and GYKI-53 provides a new perspective on the importance of a region of the ion channel for shaping the response characteristics of glutamate receptors. Strong correlations between the recent structures of AMPA receptors with and without GYKI-53 bound and the results of our single-channel studies highlight the importance of drawing on and comparing structural and functional results when designing and testing new drugs. Small structural differences within and between different subfamilies of iGluRs in the channel-gating nexus located within the LBD/channel boundary provide different substrates that may allow specific pharmacological modulation of glutamate receptors. For example, at or near its IC_{50}, the anticonvulsant drug perampanel (Fycompa; Eisai Co.), which binds to individual subunits (Yelshanskaya et al., 2016), decreases AMPA receptor channel activity by stabilizing the closed state of individual subunits, apparently without altering the behavior of adjacent subunits (Yuan et al., 2019). By comparison, small differences in the binding of GYKI-53 within the overlap site alter the dynamics of AMPA receptor channel gating by linking adjacent subunits together and introducing apparent cooperativity. Without the crystal and cryo-EM studies, important insights into both the nature of the binding site and the structural changes upon activation would be difficult to obtain. On the other hand, single-channel recordings provide detailed dynamic information not accessible by structural methods or conventional whole-cell recordings. The combination of the two, coupled with the equilibrium modeling for whole-cell data, provide a clearer picture of the function of this important class of drugs, as well as insight into an exquisitely sensitive control point on AMPA receptors that contributes to their unique functional characteristics.

References

Alsaloum, M., R. Kazi, Q. Gan, J. Amin, and L.P. Wollmuth. 2016. A Molecular Determinant of Subtype-Specific Desensitization in Ionotropic Glutamate Receptors. *J. Neurosci.* 36:2617–2622. https://doi.org/10.1523/JNEUROSCI.2667-15.2016

Arai, A.C. 2001. GYKI 52466 has positive modulatory effects on AMPA receptors. *Brain Res.* 892:396–400. https://doi.org/10.1016/S0006-8993(00)03323-0

Armstrong, N., and E. Gouaux. 2000. Mechanisms for activation and antagonism of an AMPA-sensitive glutamate receptor: crystal structures of the GluR2 ligand binding core. *Neuron.* 28:165–181. https://doi.org/10.1016/S0896-6273(00)00094-5

Armstrong, N., Y. Sun, G.Q. Chen, and E. Gouaux. 1998. Structure of a glutamate-receptor ligand-binding core in complex with kainate. *Nature.* 395:913–917. https://doi.org/10.1038/27692

Barygin, O.I. 2016. Inhibition of calcium-permeable and calcium-impermeable AMPA receptors by perampanel in rat brain neurons. *Neurosci. Lett.* 633:146–151. https://doi.org/10.1016/j.neulet.2016.09.028

Blanke, M.L., and A.M. VanDongen. 2008. The NR1 M3 domain mediates allosteric coupling in the N-methyl-D-aspartate receptor. *Mol. Pharmacol.* 74:454–465. https://doi.org/10.1124/mol.107.044115

Boulter, J., M. Hollmann, A. O'Shea-Greenfield, M. Hartley, E. Deneris, C. Maron, and S. Heinemann. 1990. Molecular cloning and functional expression of glutamate receptor subunit genes. *Science.* 249:1033–1037. https://doi.org/10.1126/science.2168579

Chen, S., Y. Zhao, Y. Wang, M. Shekhar, E. Tajkhorshid, and E. Gouaux. 2017. Activation and Desensitization Mechanism of AMPA Receptor-TARP Complex by Cryo-EM. *Cell.* 170:1234–1246.e4. https://doi.org/10.1016/j.cell.2017.07.045

Colquhoun, D., and F.J. Sigworth. 1995. Fitting and statistical analysis of single-channel recording. *In* Single-Channel Recording. Second edition. B. Sakmann, and E. Neher, editors. Plenum Press, New York. 483–585. https://doi.org/10.1007/978-1-4419-1229-9_19

Donevan, S.D., S. Yamaguchi, and M.A. Rogawski. 1994. Non-N-methyl-D-aspartate receptor antagonism by 3-N-substituted 2,3-benzodiazepines: relationship to anticonvulsant activity. *J. Pharmacol. Exp. Ther.* 271:25–29.

Gonzalez, J., M. Du, K. Parameshwaran, V. Suppiramaniam, and V. Jayaraman. 2010. Role of dimer interface in activation and desensitization in AMPA receptors. *Proc. Natl. Acad. Sci. USA.* 107:9891–9896. https://doi.org/10.1073/pnas.0911854107

Hibi, S., K. Ueno, S. Nagato, K. Kawano, K. Ito, Y. Norimine, O. Takenaka, T. Hanada, and M. Yonaga. 2012. Discovery of 2-(2-oxo-1-phenyl-5-pyridin-2-yl-1,2-dihydropyridin-3-yl)benzonitrile (perampanel): a novel, noncompetitive α-amino-3-hydroxy-5-methyl-4-isoxazolepropanoic acid (AMPA) receptor antagonist. *J. Med. Chem.* 55:10584–10600. https://doi.org/10.1021/jm301268u

Holley, S.M., A.H. Ahmed, J. Srinivasan, S.E. Murthy, G.A. Weiland, R.E. Oswald, and L.M. Nowak. 2012. The loss of an electrostatic contact unique to AMPA receptor ligand binding domain 2 slows channel activation. *Biochemistry.* 51:4015–4027. https://doi.org/10.1021/bi3001837

Klein, R.M., and J.R. Howe. 2004. Effects of the lurcher mutation on GluR1 desensitization and activation kinetics. *J. Neurosci.* 24:4941–4951. https://doi.org/10.1523/JNEUROSCI.0660-04.2004

Lomeli, H., J. Mosbacher, T. Melcher, T. Höger, J.R. Geiger, T. Kuner, H. Monyer, M. Higuchi, A. Bach, and P.H. Seeburg. 1994. Control of kinetic properties of AMPA receptor channels by nuclear RNA editing. *Science.* 266:1709–1713. https://doi.org/10.1126/science.7992055

Mitchell, N.A., and M.W. Fleck. 2007. Targeting AMPA receptor gating processes with allosteric modulators and mutations. *Biophys. J.* 92:2392–2402. https://doi.org/10.1529/biophysj.106.095091

Murthy, S.E., T. Shogan, J.C. Page, E.M. Kasperek, and G.K. Popescu. 2012. Probing the activation sequence of NMDA receptors with lurcher mutations. *J. Gen. Physiol.* 140:267–277. https://doi.org/10.1085/jgp.201210786

Nayak, P.K., and D.S. Kerr. 2013. Low-dose GYKI-52466: prophylactic preconditioning confers long-term neuroprotection and functional recovery following hypoxic-ischaemic brain injury. *Neuroscience.* 232:128–138. https://doi.org/10.1016/j.neuroscience.2012.11.063

Nicolai, C., and F. Sachs. 2013. Solving ion channel kinetics with the QuB software. *Biophys. Rev. Lett.* 8:191–211. https://doi.org/10.1142/S1793048013300053

Perszyk, R., B.M. Katzman, H. Kusumoto, S.A. Kell, M.P. Epplin, Y.A. Tahirovic, R.L. Moore, D. Menaldino, P. Burger, D.C. Liotta, and S.F. Traynelis. 2018. An NMDAR positive and negative allosteric modulator series share a binding site and are interconverted by methyl groups. *eLife.* 7:e34711. https://doi.org/10.7554/eLife.34711

Pettersen, E.F., T.D. Goddard, C.C. Huang, G.S. Couch, D.M. Greenblatt, E.C. Meng, and T.E. Ferrin. 2004. UCSF Chimera--a visualization system for exploratory research and analysis. *J. Comput. Chem.* 25:1605–1612. https://doi.org/10.1002/jcc.20084

Pøhlsgaard, J., K. Frydenvang, U. Madsen, and J.S. Kastrup. 2011. Lessons from more than 80 structures of the GluA2 ligand-binding domain in complex with agonists, antagonists and allosteric modulators. *Neuropharmacology.* 60:135–150. https://doi.org/10.1016/j.neuropharm.2010.08.004

Poon, K., L.M. Nowak, and R.E. Oswald. 2010. Characterizing single-channel behavior of GluA3 receptors. *Biophys. J.* 99:1437–1446. https://doi.org/10.1016/j.bpj.2010.06.058

Poon, K., A.H. Ahmed, L.M. Nowak, and R.E. Oswald. 2011. Mechanisms of modal activation of GluA3 receptors. *Mol. Pharmacol.* 80:49–59. https://doi.org/10.1124/mol.111.071688

Poon, K., R.E. Oswald, and L.M. Nowak. 2016. Current recording and kinetic analyses for single AMPA Receptors. In Ionotropic Glutamate Receptor Technologies. G. Popescu, editor. Humana Press, New York, NY. 257-272. https://doi.org/10.1007/978-1-4939-2812-5_17.

Prieto, M.L., and L.P. Wollmuth. 2010. Gating modes in AMPA receptors. *J. Neurosci.* 30:4449–4459. https://doi.org/10.1523/JNEUROSCI.5613-09.2010

Ptak, C.P., C.L. Hsieh, G.A. Weiland, and R.E. Oswald. 2014. Role of stoichiometry in the dimer-stabilizing effect of AMPA receptor allosteric modulators. *ACS Chem. Biol.* 9:128–133. https://doi.org/10.1021/cb4007166

Qin, F., and L. Li. 2004. Model-based fitting of single-channel dwell-time distributions. *Biophys. J.* 87:1657–1671. https://doi.org/10.1529/biophysj.103.037531

Qin, F., A. Auerbach, and F. Sachs. 1996. Estimating single-channel kinetic parameters from idealized patch-clamp data containing missed events. *Biophys. J.* 70:264–280. https://doi.org/10.1016/S0006-3495(96)79568-1

Ritz, M., C. Wang, N. Micale, R. Ettari, and L. Niu. 2011. Mechanism of Inhibition of the GluA2 AMPA Receptor Channel Opening: the Role of 4-Methyl versus 4-Carbonyl Group on the Diazepine Ring of 2,3-Benzodiazepine Derivatives. *ACS Chem. Neurosci.* 2:506–513. https://doi.org/10.1021/cn200033j

Rogawski, M.A. 2011. Revisiting AMPA receptors as an antiepileptic drug target. *Epilepsy Curr.* 11:56–63. https://doi.org/10.5698/1535-7511-11.2.56

Rogawski, M.A., and T. Hanada. 2013. Preclinical pharmacology of perampanel, a selective non-competitive AMPA receptor antagonist. *Acta Neurol. Scand. Suppl.* 127:19–24. https://doi.org/10.1111/ane.12100

Rosenmund, C., Y. Stern-Bach, and C.F. Stevens. 1998. The tetrameric structure of a glutamate receptor channel. *Science.* 280:1596–1599. https://doi.org/10.1126/science.280.5369.1596

Sigworth, F.J., and S.M. Sine. 1987. Data transformations for improved display and fitting of single-channel dwell time histograms. *Biophys. J.* 52:1047–1054. https://doi.org/10.1016/S0006-3495(87)83298-8

Silberberg, S.D., A. Lagrutta, J.P. Adelman, and K.L. Magleby. 1996. Wanderlust kinetics and variable Ca^{2+}-sensitivity of dSlo, a large conductance CA^{2+}-activated K^+ channel, expressed in oocytes. *Biophys. J.* 71:2640–2651. https://doi.org/10.1016/S0006-3495(96)79833-8

Smith, T.C., and J.R. Howe. 2000. Concentration-dependent substate behavior of native AMPA receptors. *Nat. Neurosci.* 3:992–997. https://doi.org/10.1038/79931

Sobolevsky, A.I., M.P. Rosconi, and E. Gouaux. 2009. X-ray structure, symmetry and mechanism of an AMPA-subtype glutamate receptor. *Nature.* 462:745–756. https://doi.org/10.1038/nature08624

Sommer, B., K. Keinänen, T.A. Verdoorn, W. Wisden, N. Burnashev, A. Herb, M. Köhler, T. Takagi, B. Sakmann, and P.H. Seeburg. 1990. Flip and flop: a cell-specific functional switch in glutamate-operated channels of the CNS. *Science.* 249:1580–1585. https://doi.org/10.1126/science.1699275

Sun, Y., R. Olson, M. Horning, N. Armstrong, M. Mayer, and E. Gouaux. 2002. Mechanism of glutamate receptor desensitization. *Nature.* 417:245–253. https://doi.org/10.1038/417245a

Talukder, I., P. Borker, and L.P. Wollmuth. 2010. Specific sites within the ligand-binding domain and ion channel linkers modulate NMDA receptor gating. *J. Neurosci.* 30:11792–11804. https://doi.org/10.1523/JNEUROSCI.5382-09.2010

Talukder, I., R. Kazi, and L.P. Wollmuth. 2011. GluN1-specific redox effects on the kinetic mechanism of NMDA receptor activation. *Biophys. J.* 101:2389–2398. https://doi.org/10.1016/j.bpj.2011.10.015

Taverna, F., Z.G. Xiong, L. Brandes, J.C. Roder, M.W. Salter, and J.F. MacDonald. 2000. The Lurcher mutation of an alpha-amino-3-hydroxy-5-methyl-4-isoxazolepropionic acid receptor subunit enhances potency of glutamate and converts an antagonist to an agonist. *J. Biol. Chem.* 275:8475–8479. https://doi.org/10.1074/jbc.275.12.8475

Twomey, E.C., and A.I. Sobolevsky. 2018. Structural Mechanisms of Gating in Ionotropic Glutamate Receptors. *Biochemistry.* 57:267–276. https://doi.org/10.1021/acs.biochem.7b00891

Twomey, E.C., M.V. Yelshanskaya, R.A. Grassucci, J. Frank, and A.I. Sobolevsky. 2017. Channel opening and gating mechanism in AMPA-subtype glutamate receptors. *Nature.* 549:60–65. https://doi.org/10.1038/nature23479

Wang, C., Y. Han, A. Wu, S. Sólyom, and L. Niu. 2014. Mechanism and site of inhibition of AMPA receptors: pairing a thiadiazole with a 2,3-benzodiazepine scaffold. *ACS Chem. Neurosci.* 5:138–147. https://doi.org/10.1021/cn400193u

Wo, Z.G., and R.E. Oswald. 1995. Unraveling the modular design of glutamate-gated ion channels. *Trends Neurosci.* 18:161–168. https://doi.org/10.1016/0166-2236(95)93895-5

Wu, A., C. Wang, and L. Niu. 2014. Mechanism of inhibition of the GluA1 AMPA receptor channel opening by the 2,3-benzodiazepine compound GYKI 52466 and a N-methyl-carbamoyl derivative. *Biochemistry.* 53:3033–3041. https://doi.org/10.1021/bi5002079

Yelshanskaya, M.V., A.K. Singh, J.M. Sampson, C. Narangoda, M. Kurnikova, and A.I. Sobolevsky. 2016. Structural Bases of Noncompetitive Inhibition of AMPA-Subtype Ionotropic Glutamate Receptors by Antiepileptic Drugs. *Neuron.* 91:1305–1315. https://doi.org/10.1016/j.neuron.2016.08.012

Yelshanskaya, M.V., S. Mesbahi-Vasey, M.G. Kurnikova, and A.I. Sobolevsky. 2017. Role of the Ion Channel Extracellular Collar in AMPA Receptor Gating. *Sci. Rep.* 7:1050. https://doi.org/10.1038/s41598-017-01146-z

Yuan, C.L., E.Y. Shi, J. Srinivasan, C.P. Ptak, R.E. Oswald, and L.M. Nowak. 2019. Modulation of AMPA receptor gating by the anticonvulsant drug, Perampanel. *ACS Med. Chem. Lett.* 10:. https://doi.org/10.1021/acsmedchemlett.8b00322

Zhang, W., S.P. Devi, S. Tomita, and J.R. Howe. 2014. Auxiliary proteins promote modal gating of AMPA- and kainate-type glutamate receptors. *Eur. J. Neurosci.* 39:1138–1147. https://doi.org/10.1111/ejn.12519

Zhang, W., C. Eibl, A.M. Weeks, I. Riva, Y.J. Li, A.J.R. Plested, and J.R. Howe. 2017. Unitary Properties of AMPA Receptors with Reduced Desensitization. *Biophys. J.* 113:2218–2235. https://doi.org/10.1016/j.bpj.2017.07.030

Zuo, J., P.L. De Jager, K.A. Takahashi, W. Jiang, D.J. Linden, and N. Heintz. 1997. Neurodegeneration in Lurcher mice caused by mutation in delta2 glutamate receptor gene. *Nature.* 388:769–773. https://doi.org/10.1038/42009

Shi et al.
Antagonist-induced cooperative AMPA receptor gating

Journal of General Physiology 173
https://doi.org/10.1085/jgp.201812209